Answer to Referee Comment 1

July 10, 2018

We thank referee 1 for valuable comments and suggestions. Our answers are given below. The original referee comment is repeated in **bold**, changes in the manuscript text are printed in *italic.*

TECHNICAL CORRECTIONS:

The statement "Space-borne measurements provide global coverage" (pag. 2, line 9) is not necessarily true. Geostationary satellites do not provide global coverage. I suggest the following modification: "Space-borne measurements can provide global coverage"
We changed the manuscript according to the referee's suggestion.

The detailed description of the results from a single flight from the PGS campaign was performed by selecting flight PGS-19. Is that the result of a purely random choice or of a selection based on pre-established criteria? A short statement providing this information to the reader might be of help.
We added the following sentence in Sec. 4, to briefly motivate the selection of flight PGS19 for detailed analysis: *Flight PGS19 is selected as an example of continuous measurements in high spectral resolution mode, and as an example of an illustrative amount of atmospheric variability within the measured air masses.*

The term "combination" (suggesting a synergistic use of data) referred to the link established between GLORIA and MLS data does not appear the most appropriate. The extent to which the two datasets were jointly used to build the results reported in the

manuscript appears to be rather limited. The term "comparison" might still be more appropriate to represent the actual exercise conducted using both data sets. I leave to the authors to decide on this point.
We changed the term to *comparison* according to the referee's suggestion.

If available from the diagnostics of GLORIA measurements during the PGS campaign (or the PGS-19 flight): which is the typical amount of bad pixels filtered out (per row or per image)? Is that affecting the quality of the measurements in a significant manner with margins for future improvements?
The amount of bad pixels is in the order of 5 to 10%. The bad pixel filtering should not significantly degrade the retrieval result, as the noise error only plays a minor role (see Fig. 4). We change the text in Sec. 2.1 to: *For noise reduction, the pixels of each detector row are averaged after filtering of bad pixels (typically 5 to 10%).*

In the statement "Another important quantity for a retrieval is the degrees of freedom" (pag.9, line 26), the correct expression to use is "the number of degrees of freedom".
We changed the manuscript according to the referee's suggestion.

The statement "... since the diagonal element of each averaging kernel row is a measure ... retrieval results" (pag. 9, line 27) shall be formulated in a different manner, to avoid using the expression "diagonal element of a row".
We change the formulation to: *... since the diagonal elements of the averaging kernel are measures of how much measurement information is contained in the retrieval result per level.*

We also thank referee 1 for the detailed language corrections, which helped us to further improve the manuscript.

Answer to Referee Comment 2

July 10, 2018

We thank referee 2 for valuable comments and suggestions. Our answers are given below. The original referee comment is repeated in **bold**, changes in the manuscript text are printed in *italic*.

TECHNICAL CORRECTIONS:
[1/13] "... differences are mainly within the expected performance" "Event with stronger deviations are explained ... ". You need to quantify where you set the threshold between what you consider an "acceptable" overlap, and the onset of "unfavourable conditions" which consequentially prohibit a direct comparison. (On a sidenote, "mostly" would be better than "mainly" as you're describing a countable factor, but in general phrases like "mostly, mainly, or more or less" should be avoided in a scientific paper if at all possible.
We changed the text to: *73% of these differences are within twice the combined estimated errors of the cross-compared instruments. Events with larger deviations ..*
We also add a temperature/trace gas specific statement in Sec. 4.4: *Another measure for the agreement between GLORIA and in-situ instruments is the part of co-located measurements, of which the differences are within twice the combined estimated errors of the cross-compared instruments. For temperature 88%, for* HNO_3 *73%, for* O_3 *63%, for* $ClONO_2$ *53%, for* H_2O *90%, for CFC-12 77%, and in total 73% of the comparisons show this agreement.* $ClONO_2$*,* O_3*, and* HNO_3 *show substantial variations at flight altitude (e.g. Figs. 9,8,7). We attribute the lower fraction of agreement to the higher atmospheric variability of those trace gases, thereby complicating the comparison due to the strongly differing instrumental sampling characteristics.*

[2/10] "Space-borne measurements ... are limited in sampling and accuracy". Maybe say: "Current space-borne measurements ... " to acknowledge the next generation of instrument, i.e. AtmoSat that will do much better.
We changed the manuscript according to the referee's suggestion.

[2/28] " ... showed reasonable agreement ...". Again, be specific. What does 'reasonable' mean, and how does the 'stage of development' affect this?
The Woiwode et al., 2015 paper is describing results from the first GLORIA field campaign. As for most newly constructed instruments, technical improvements were implemented after an analysis of the first results. The most impact on data quality had modifications to reduce the aero-acoustical properties of aircraft and interferometer. We changed the text towards a more specific formulation: *..., showed an agreement with MIPAS-STR and in-situ instruments, within the profile-to-profile variations of GLORIA. After this campaign, aero-acoustical modifications of the aircraft and of the GLORIA instrument improved the precision of GLORIA measurements.*

[3/2] "The scientific objectives ... ". This sentence/list is too long. It gets confusing. Why not write: "Among the scientific objectives of PSG campaign are: ... ; ... ; ... ; and ... Importantly, there should be a comma after "chlorine de-/activation[,] and de-/nitrification" or else the sentence implies that there is "chlorine de-/nitrification".
We changed the manuscript according to the referee's suggestion.

[3/14] "... corresponds to a displacement of the carrier ... ". Don't call the aircraft a carrier, call it the "aircraft", or the "platform". The expression 'displacement of the carrier' could be confused with the movement of carrier for the roof mirror inside your FTS instrument.
We changed from *carrier* to *platform*.

[4/25] "... onto the correct abscissa in space.". I don't understand this. Is this to correct for spherical aberration in a Gauss beam?

Compared to the on-axis beam, the optical path difference (OPD) is shorter for radiation passing through the interferometer under an off-axis angle alpha: OPD(alpha)=OPD(0)*cos(alpha). Since the off-axis angle is different for each detector pixel on the array, the different OPD must be taken into account during the level 1 processing. We change the text to: *... and the optical path difference of each pixel is determined according to its off-axis angle, in order to sample each interferogram onto the correct abscissa in space.*

[4/27] "... different temperatures.". What temperatures? Are you using cooled, heated or ambient targets? The temperature differences between the calibration targets, and their relation to the Brightness Temperature in the limb will affect your calibration errors (mainly the gain).

The black-bodies can be either cooled or heated. In order to avoid ice contamiation, the cold black-body is kept only a few Kelvin below ambient temperature, while the hot black-body is heated to 30 to 40 K above the cold one. the higher radiance compared to the limb measurements is compensated by a lower integration time. We add a reference for the blackbodies and change the text to: *Gain and offset are determined from regular in-flight measurements of the two on-board black-bodies (Olschewski et al., 2013). The temperature difference between the two black-bodies is about 30 to 40 K with the cold black-body being around or slightly below ambient temperature.*

Olschewski, F., Ebersoldt, A., Friedl-Vallon, F., Gutschwager, B., Hollandt, J., Kleinert, A., Monte, C., Piesch, C., Preusse, P., Rolf, C., Steffens, P., and Koppmann, R.: The in-flight blackbody calibration system for the GLORIA interferometer on board an airborne research platform, Atmos. Meas. Tech., 6, 3067-3082, https://doi.org/10.5194/amt-6-3067-2013, 2013.

[4/Fig.1] The colours in the legend are unclear. I.e. I can't tell PSG19-21 apart, which is critical because PSG 19 is your main flight. Also, on the legend there are at least 4 flights in different hues fo blue, but I can only see 1 blue track on the map. Incidentally, you also refer to flight PSG 12 on several occasions in the paper (i.e. Fig.2) so you should probably highlight this one as well on the map.

It is difficult to find 17 colors, which are easy to distinguish for everyone, as colors are not perceived in the same way by different persons. Still, we tried a different approach with a color selection suggested by `https://`

`sashat.me/2017/01/11/list-of-20-simple-distinct-colors/` (checked 3 July 2018). We also highlighted flight PGS12 on the map as suggested.

[5/17] "... a precision of 0.7% x VMR +/- 0.35ppmv". I'm not sure this makes sense. In a format X +/- Y, Y is the "precision", so how can you have a value for precision that has itself a precision attached to it? I guess you're talking about a statistical analysis of an ensemble of measurement precisions. If so maybe worth to clarify.
The precision of the FISH instrument is estimated with a relative part (0.7% × VMR) and an absolute part (0.35 ppmv). We changed the manuscript to avoid the misleading +/- notation and to clarify: *FISH ... achieved a precision of 0.7% × vmr (volume mixing ratio; relative part of the precision) + 0.35 ppmv (absolute part of the precision) ... during PGS.*

[5/30] "precision of X and an uncertainly of Y". Again, same as above: "uncertainly" = "precision"
We replaced *uncertainty* by *accuracy (based on systematic errors)* in this sentence.

[6/22] "... radiation transfer model ... optimized for highly resolves spectra". I think they are generally called "radiative" transfer models. Also, the spectral resolution of a RTM is usually constrained by computational resources alone, not the algorithm, so I don't understand how the RTM can be "optimized" for high resolution.
We changed the text to: *..., which is optimized for computationally efficient analyses of highly resolved spectral measurements.*

[7/9] "... a constant (H2O) profile of 10ppmv is used". Even in the Troposphere? That could have a big impact on your simulated radiances because it would significantly change the opacity at the far end of your pencil beam (Tropospheric 'continuum').
We have tested this approach in comparison with the use of more realistic initial guess profiles from ecmwf. The main effect was a larger number of iterations, but the retrieval results differed only within the estimated errors. Still we decided to use the constant initial guess and invest this larger number of iterations to be sure that any features in the retrieved profiles are not

imposed by the initial guess. We added to the sentence: *... , a constant profile of 10 ppmv is used as initial guess, in order to assure independence of derived vertical and horizontal structures in the water vapor distribution e.g. compared to initial guess profiles from meteorological analysis.*

[7/16] "calibration errors" and "pointing errors" are listed twice.
Thank you for pointing that out. We removed the repetitions.

[9/7] "With this method ... ". I find this entire sentence confusing. Radiometric calibration errors are not attributed to gain and offset, but they result in gain and offset errors. They are attributed to things like errors in temperature knowledge, non-blackbody emissivities, standing waves, etc.
We changed this sentence to: *With this method, uncertainties in the radiometric calibration are calculated considering uncertainties in the multiplicative gain of 2% and uncertainties in the additive radiance offset of 50.0* $nWcm^{-2}sr^{-1}cm$.

[9/9] "LOS errors are estimated ... ". Again, I don't fully understand what you did here. This is important, as the handling of LOS errors are a dominant error source according to you, so it needs to be crystal clear how they have been handled. (i.e. is the 0.05deg perturbation the variance of all unperturbed profile retrievals?)
The estimation of the 0.05° LOS perturbation is based on the short-term variance (not the long term changes!) of the LOS retrievals on a profile-to-profile basis (see Fig. 5b) and uncertainties within the retrieval itself. We changed the text to: *LOS errors are estimated by retrievals assuming a 0.05° LOS offset. This estimation is based on the short-term profile-to-profile variability found in the LOS retrievals (see Sec. 4.3.1), and systematic uncertainties inherent to the LOS retrieval, such as uncertainties in ECMWF atmospheric temperature and pressure.*

[9/13] "... the related temperature error". I presume this is the T error in the ECMW data?
For trace gas retrievals, the retrieved temperature is used and thus also the temperature error related to this retrieved temperature. To clarify, we added: *... related temperature error (estimated for the temperature retrieval).*

[9/28] "... the diagonal element of each averaging kernel row ... ". This is an incorrect definition of the degrees of freedom in the retrieval. To start with, a vector (AVK row) can't have a diagonal element per definition. Please review!
We change the formulation to: *... since the diagonal elements of the averaging kernel are measures of how much measurement information is contained in the retrieval result per level.*

[10/16] "This stop allowed for higher altitudes of the HALO aircraft...". It's not the stop that makes the plane fly higher. How about: "HALO reaches its peak ceiling altitude immediately before each refuelling stop, when the airframe is at its lightest. It's only at these phases of the flight that the flight altitude is high enough to sample subsided polar ... ".
We changed the manuscript according to the referee's suggestion.

[12/Fig.3] The flight track in the vicinity of waypoints A and B is not very visible. Could you use lighter colours?
We changed the figure, such that the magenta flight track is put one layer above the white/transparent background of the way point labels to increase contrast at this region. At least in panel (a) the flight path is now easily visible, for panels (b)-(d) the contrast still is somewhat lower due to the red colors of the shown meteorological/trace gas quantity. Still magenta is one of the few colors not included in the used colormap.

[13/Fig.4] The axes of panels c) and f) (vertical resolution) should be capped at 1.5km (or even 1km instead of 3.0km. This would better resolve the profile variations at the altitudes that actually matter.
We changed the figure according to the referee's suggestion.

[14/2] "... caused by changes in the atmospheric state ... ". Why is that? Changes in refracted path if the temperature/density is incorrect?
We clarify by stating the influence of temperature to the spectra of CO_2, which is also used for the LOS retrieval: *This difference in the retrieved*

LOS can be caused by differences in the atmospheric state compared to the ECMWF fields (which also affects the intensity of the CO_2 spectral lines, that are used for the LOS retrieval), ...

[14/8] "For flights between ... " and following sentences: I think I understand what you are saying, but I had to read this section many times over before it became clear to me. Could you rephrase it in a less convoluted way?
We added a close-up of some of the discussed drifts and jumps in Fig. 5 to show the problem in a more detailed way. We extended the paragraph to: *For flights between 21 December 2015 and 31 January 2016 a software malfunction of the pointing control software caused the LOS to drift away from the commanded elevation. At certain points the software changed the instrument elevation back to its correct value and steep steps in the retrieved pointing elevation angle are observed in these flights (see Fig. 5a, enlargement: "Drift" and "Jump"). A correction of this artifact can be calculated by interpolating the LOS between the points immediately after a steep step. This interpolated line between the correct elevation angles approximates the LOS that would have been retrieved for a measurement without this software malfunction. The same average LOS correction, which is used for other flights, can be calculated from this interpolated LOS (Fig. 5a, green points). This is the first part of the LOS correction for these flights. In the second part, the influence of the software malfunction can be extracted by subtraction of the interpolated LOS from the retrieved LOS. For an idealized measurement (without any further error in the LOS), this method separates the effect of the software malfunction from long-term variations (which have been corrected for in the first part). For subsequent retrievals of temperature and volume mixing ratios, both corrections, the average LOS correction and the correction of the steps, have been applied (Fig. 5a, red points).*

[15/Fig. 5]: I can't tell the dark blue and the black dots apart in my A4 printout. Please use high contrast colours, i.e. red and black.
We changed the figure according to the referee's suggestion.

[17/4] "This is the same regions, where the HNO3 ... ". I have the impression that the HNO3 mismatch peaks at 17:00h, while the O3 mismatch peaks at 16:00h. Is that really the same air-parcel? On

the same note: Why are AIMS and FAIRO comparisons plotted on what are really quite different time-scales in their respective panels.

We adjusted all figures including in-situ comparisons to the same time-axis as for the GLORIA plots. The difference in the previous plots was caused by different data availability for each in-situ instrument, but we agree that for a better comparison the same time axis should be used.

With the newly adjusted time axis, it can be easier seen, that structures in HNO_3 and O_3 show similarities (for GLORIA and in-situ). For both trace gases, there is a decrease at 16:00 in GLORIA measurements, which is not seen in the in-situ data and also for both trace gases the structures shortly before 17:00 are reproduced by GLORIA. The amplitude of these structures show larger differences between remote sensing and in-situ for HNO_3 compared to O_3.

[18/?] "Baffin Bay". Where is Baffin Bay located in Fig 3? Not really common knowledge.

We clarified by adding to the text: *... Baffin Bay (the region covered by the GLORIA tangent points between way points "A" and "B"; ....*

[18/?] General comment to this paragraph: You really should mention the good agreement between spatial features observed in O3 and HNO3. This is what you would expect from atmospheric chemistry, and the fact that you actually see it is an important self-validation of your results!

We add the following part to the paragraph: *Spatial features are in agreement with the ones observed in HNO_3 (see Fig. 7), which is expected from atmospheric chemistry (Popp et al., 2009). This close correlation between the GLORIA measurements of both trace gases is an additional self-check for the validity of our results.*

Popp, P. J., et al. (2009), Stratospheric correlation between nitric acid and ozone, J. Geophys. Res., 114, D03305, doi: 10.1029/2008JD010875

[18/7] "... subsided deactivated ClONO2". A large presence of the reservoir gas ClONO2 is a sign of "deactivated" ClO, and should therefore probably be called "activated" ClONO2.

We changed the text to: *... subsided deactivated chlorine in form of $ClONO_2$.*

[21/22] "... numerous flights in January 2016, which have been affected by PSCs ... ". This merit a separate Figure, and a short paragraph. It constitutes a separate, unique scientific finding of the campaign. Because the paper is aiming to be the reference publication of all flight in PSG, this should not be demoted to a mere side-not, just because it's not visible in the example flight PGS 19. You make a reference to a "supplement" that contains these additional plots, which I presume are part of the special edition, but I don't have access to this supplement, and neither will anyone that downloads your article as a standalone document form a research database a few years down the line. To make the paper useful in the long term, this link should either be omitted, or at the very least you will have to reference it (with full DOI information) in the text.

In Fig. 2a, flight PGS12 is shown as an example for a PSC affected flight. This was reported by the flight crew and is visible in the lower Cloud-Index values close to flight altitude. Still the CI does not proof the existence of PSCs, it only gives a measure for the cloudiness along the limb, which affects the trace gas retrievals. For a detailed PSC analysis, more advanced retrieval methods are necessary (e.g. Spang et al., 2016), which are out of the scope of the paper. Pitts et al. (2018) also give an overview of PSCs measured by CALIOP and the extension of PSCs down to lower altitudes in the 2015/16 Arctic winter are visible in his work.

To clarify, we change the text to: *... numerous flights in January 2016, which have been strongly affected by PSCs at and above flight level. From the HALO flight crew, PSCs have been reported at these altitudes for PGS flights until PGS14 (26 February 2016). The influence of PSC and high altitude cirrus clouds on the spectra are shown in Fig. 2a as lower CI values at and below flight altitude.*

The supplement is publicly available via the AMTD website of this article: `https://www.atmos-meas-tech-discuss.net/amt-2018-52/amt-2018-52-supplement.pdf`. According to Copernicus Publications, a DOI would be assigned to the supplement during the typesetting process in case of a publication in AMT.

Pitts, M. C., Poole, L. R., and Gonzalez, R.: Polar stratospheric cloud climatology based on CALIPSO spaceborne lidar measurements from 20062017, Atmos. Chem. Phys. Discuss., https://doi.org/10.5194/acp-2018-234, in review, 2018.

Spang, R., Hoffmann, L., Höpfner, M., Griessbach, S., Müller, R., Pitts, M.

C., Orr, A. M. W., and Riese, M.: A multi-wavelength classification method for polar stratospheric cloud types using infrared limb spectra, Atmos. Meas. Tech., 9, 3619-3639, https://doi.org/10.5194/amt-9-3619-2016, 2016.

[23/17] "This lower resolution does not resolve spatially confined enhancements in these trace gases." MLS is still sensitive to the filament enhancements, even if it can't resolve them. If you re-grid the data carefully, i.e. by applying the MLS averaging kernels to your measurements, the observed VMR values should match. Are you comparing the peak VMR values from a high vertical resolution IR measurements with a low vertical resolution MSR measurement? In this case, the discrepancy is indeed to be expected, but it's not strictly because the MLS can't see it, but because the MLS measurements contains information from (O3-depleted) polar stratospheric air. So, you're comparing apples with pears.
Unfortunately we have to stay with this more descriptive analysis since a quantitative comparison by applying the MLS AKs to the GLORIA measurements is not possible since GLORIA does not provide altitude resolved information above the flight level - where MLS AKs still have major contributions. In order to clarify, we change to: *This lower resolution does not resolve spatially confined enhancements in these trace gases. Due to only partial overlap of vertically resolved information from GLORIA and the width of the MLS averaging kernels, it is not possible to perform a more quantitative comparison.*

[23/13] "... which is lower compared to ... previous IR limb sounders". Why is that?
We add to the sentence: *... which is lower compared to the majority of previously discussed infrared limb sounders, due to the much higher vertical and horizontal sampling of the limb-imaging spectrometer.*

[23/17] Again, "rather" is a very meek and unspecific term. Your closing sentence should have some clout. How about: "GLORIA measurements with unprecedented spatial resolution over the Arctic region will form the basis for many future case studies on ... "
We changed the manuscript according to the referee's suggestion. Thanks for this excellent suggestion!

We also thank referee 2 for the detailed formal corrections. We applied most of these suggestions, which helped us to further improve the manuscript.

Airborne limb-imaging measurements of temperature, HNO_3, O_3, $ClONO_2$, H_2O and CFC-12 during the Arctic winter 2015/16: ~~characterization~~Characterization, in-situ validation and comparison to Aura/MLS

Sören Johansson[1], Wolfgang Woiwode[1], Michael Höpfner[1], Felix Friedl-Vallon[1], Anne Kleinert[1], Erik Kretschmer[1], Thomas Latzko[1], Johannes Orphal[1], Peter Preusse[2], Jörn Ungermann[2], Michelle L. Santee[3], Tina Jurkat-Witschas[4], Andreas Marsing[4], Christiane Voigt[4], Andreas Giez[5], Martina Krämer[2], Christian Rolf[2], Andreas Zahn[1], Andreas Engel[6], Björn-Martin Sinnhuber[1], and Hermann Oelhaf[1]

[1] Institute of Meteorology and Climate Research, Karlsruhe Institute of Technology, Karlsruhe, Germany
[2] Institute of Energy and Climate Research - Stratosphere (IEK-7), Forschungszentrum Jülich, Jülich, Germany
[3] Jet Propulsion Laboratory, California Institute of Technology, Pasadena, California, USA
[4] Institute of Atmospheric Physics, Deutsches Zentrum für Luft- und Raumfahrt, Oberpfaffenhofen, Germany
[5] Flight Experiments, Deutsches Zentrum für Luft- und Raumfahrt, Oberpfaffenhofen, Germany
[6] Institute for Atmospheric and Environmental Sciences, Goethe-University Frankfurt, Frankfurt, Germany

Correspondence to: S. Johansson (soeren.johansson@kit.edu)

Abstract. The Gimballed Limb Observer for Radiance Imaging of the Atmosphere (GLORIA) was operated on board the German High Altitude and LOng range (HALO) research aircraft during the PGS (POLSTRACC/GW-LCYCLE/SALSA) aircraft campaigns in the Arctic winter 2015/2016. Research flights were conducted from 17 December 2015 until 18 March 2016 between 80°W - 30°E longitude and 25°N - 87°N latitude. From the GLORIA infrared limb emission measurements, two dimensional cross sections of temperature, HNO_3, O_3, $ClONO_2$, H_2O and CFC-12 are retrieved. During 15 scientific flights of the PGS campaigns the GLORIA instrument measured more than ~~15000~~ 15'000 atmospheric profiles at high spectral resolution. Dependent on flight altitude and tropospheric cloud cover, the profiles retrieved from the measurements typically range between 5 and 14 km, and vertical resolutions between 400 m and 1000 m are achieved. The estimated total (random and systematic) 1-σ errors are in the range of 1 to 2 K for temperature and 10 % to 20 % relative error for the discussed trace gases. Comparisons to in-situ instruments deployed on board HALO have been performed. Over all flights of this campaign the median differences and median absolute deviations between in-situ and GLORIA observations are -0.75 K ± 0.88 K for temperature, -0.03 ppbv ± 0.85 ppbv for HNO_3, -3.5 ppbv ± 116.8 ppbv for O_3, -15.4 pptv ± 102.8 pptv for $ClONO_2$, -0.13 ppmv ± 0.63 ppmv for H_2O and -19.8 pptv ± 46.9 pptv for CFC-12. ~~These differences are mainly within the expected performances~~ 73% of these differences are within twice the combined estimated errors of the cross-compared instruments. Events with ~~stronger~~ larger deviations are explained by atmospheric variability and different sampling characteristics of the instruments. Additionally, comparisons of GLORIA HNO_3 and O_3 with measurements of the Aura Microwave Limb Sounder

(MLS) instrument show highly consistent structures in trace gas distributions and illustrate the potential of the high spectral resolution limb-imaging GLORIA observations for resolving narrow mesoscale structures in the UTLS.

1 Introduction

The ~~region of the upper troposphere and lower stratosphere~~ Upper Troposphere and Lower Stratosphere (UTLS) is a key region for climate on Earth (Gettelman et al., 2011). The extra-tropical UTLS is influenced by vertical downward transport from the stratosphere by the Brewer-Dobson circulation, by horizontal transport from the upper tropical troposphere by isentropic mixing, by convective overshooting and mixing with the troposphere (Holton et al., 1995; Bönisch et al., 2011). The UTLS is challenging to observe. Isentropic mixing in this region happens via very long filaments with small vertical and horizontal extent (Konopka and Pan, 2012). This requires a large horizontal coverage on the one-hand and high spatial resolution on the other hand. Aircraft infrared limb-emission measurements can fill the gap between airborne in-situ instruments and space-borne remote sensing satellites. Airborne in-situ instruments provide a high accuracy, high temporal resolution and along-track sampling, but they are limited to the vertical and horizontal dimensions of the aircraft's flight track. ~~Space-borne measurements~~ Current space-borne measurements can provide global coverage but are limited in terms of spatial sampling and accuracy. Aircraft and balloon measurement campaigns with infrared limb-emission remote sensing instruments have been a source of vertically, spatially and/or temporally resolved observations of temperature and a wealth of trace gases (e.g. Piesch et al., 1996; Friedl-Vallon et al., 2004) as well as important steps for demonstration of technology for future satellite missions (e.g. Fischer et al., 2008).

The ~~Gimballed Limb Observer for Radiance Imaging of the Atmosphere (GLORIA)~~ GLORIA instrument (Friedl-Vallon et al., 2014) continues the heritage of the series of MIPAS (Michelson Interferometer for Passive Atmospheric Sounding (Fischer and Oelhaf, 1996; Piesch et al., 1996; Friedl-Vallon et al., 2004)) and CRISTA (CRyogenic Infrared Spectrometers and Telescopes for the Atmosphere (Offermann et al., 1999; Ungermann et al., 2012)) instruments. One major improvement of GLORIA compared to its limb-scanning precursors is the usage of an imaging array detector for significantly higher spatial sampling and precise relative pointing. A wider overview of scientific objectives for these altitudes and the potential of the GLORIA instrument for such science questions is given by Riese et al. (2014).

Measurements with the airborne MIPAS-STR (MIPAS- STRatospheric aircraft) instrument provided precise and accurate temperature and trace gas profiles (Woiwode et al., 2012). The GLORIA measurements aim for significantly higher vertical resolutions. Due to the higher spatial sampling along the flight track, a larger set of profiles is measured. Ungermann et al. (2015) discussed and validated GLORIA temperature, H_2O, HNO_3 and O_3 retrievals from the GLORIA high spatial resolution mode. Woiwode et al. (2015) described the first GLORIA high spectral resolution observations captured in 2011 during the ESSenCe (ESA Sounder Campaign) campaign. They compared temperature, HNO_3, O_3, H_2O, CFC-11 and CFC-12 profiles with in-situ profiles and MIPAS-STR collocated profiles, and they found that GLORIA, at this stage of development, showed ~~reasonable~~ an agreement with MIPAS-STR and in-situ instruments~~.~~, within the profile-to-profile variations of GLORIA. After this campaign, aero-acoustical modifications of the aircraft and of the GLORIA instrument improved the precision of GLORIA measurements.

Here, a much higher number of profiles was measured, the instrument has been technically improved, $ClONO_2$ is presented as additional trace ~~gases~~ gas and the results at flight altitude are compared to in-situ observations from the same platform HALO (High Altitude and LOng range aircraft). Additionally a first ~~combination~~ comparison of GLORIA and Aura/MLS (Microwave Limb Sounder) data is presented.

The PGS mission is the combination of the POLSTRACC (POLar STRAtosphere in a Changing Climate) aircraft campaign (Oelhaf et al., 2015) together with GW-LCYCLE II (Gravity Wave Life Cycle Experiment) and SALSA (Seasonality of Air mass transport and origin in the Lowermost Stratosphere using the HALO Aircraft) campaigns. The combined mission took place in the Arctic winter 2015/2016 with bases in Oberpfaffenhofen (Germany) and Kiruna (Sweden). ~~The~~ Among the scientific objectives of ~~the~~ PGS campaign are~~among others to investigate~~: investigation of chemical processes such as ozone depletion, chlorine ~~de-/activation and de-/nitrification~~ de-activation, and de-nitrification in the lowermost stratosphere~~as well as~~; mixing and dynamical linkages between the upper troposphere, the lower stratosphere, and between high latitudes and middle latitudes over the course of the winter; and gravity waves. For that purpose, nine in-situ and three remote sensing instruments probed the UTLS region during 18 HALO research flights between December 2015 and March 2016. The flight paths are shown in Fig. 1. These 18 PGS research flights, each with a duration of approximately 10 hours, cover the whole time of the Arctic winter and provide ~~with HALO flights of typically 10 hours of duration~~ a unique data set.

The goal of the paper in hand is to characterize and validate the GLORIA observations during the course of the Arctic winter, involving measurements under cloud-free conditions and conditions affected by polar stratospheric clouds (PSCs). The data product is characterized considering random and systematic errors, and an approach for correcting systematic line-of-sight errors in limb-imaging observations is presented. Finally, the GLORIA observations are brought into a broader perspective by comparisons with Aura/MLS observations and demonstrate the capability of GLORIA of resolving mesoscale structures in the UTLS. This paper shall provide the baseline and reference for scientific studies using GLORIA measurements.

2 Instruments

2.1 GLORIA

The essential parts of the GLORIA instrument (Friedl-Vallon et al., 2014, and the AMT special issue this paper belongs to) are an imaging spectrometer, a gimballed frame for pointing and line-of-sight stabilization and two black-bodies for radiometric calibration. The spectrometer is a Fourier Transform Spectrometer (FTS) with a HgCdTe infrared detector array. 48 × 128 (horizontal × vertical) pixels of this imaging detector are used to record the same number of interferograms simultaneously. In order to reduce thermal noise, the spectrometer is cooled down to -50°C (Piesch et al., 2015). Depending on the scientific goals, the GLORIA spectrometer can be operated in two different measurement modes: The high spatial resolution mode with a spectral sampling of 0.625 cm^{-1} and a temporal resolution of 2 s and the high spectral resolution mode with a sampling of 0.0625 cm^{-1} and 13 s. In this paper, results of measurements in high spectral resolution are discussed. In this measurement, configuration 48 × 128 interferograms are recorded every 13 s, which corresponds to displacement of the ~~carrier~~ platform of ≈3 km considering typical HALO cruise speed. The gimbal frame is used to compensate for the movements of the carrying

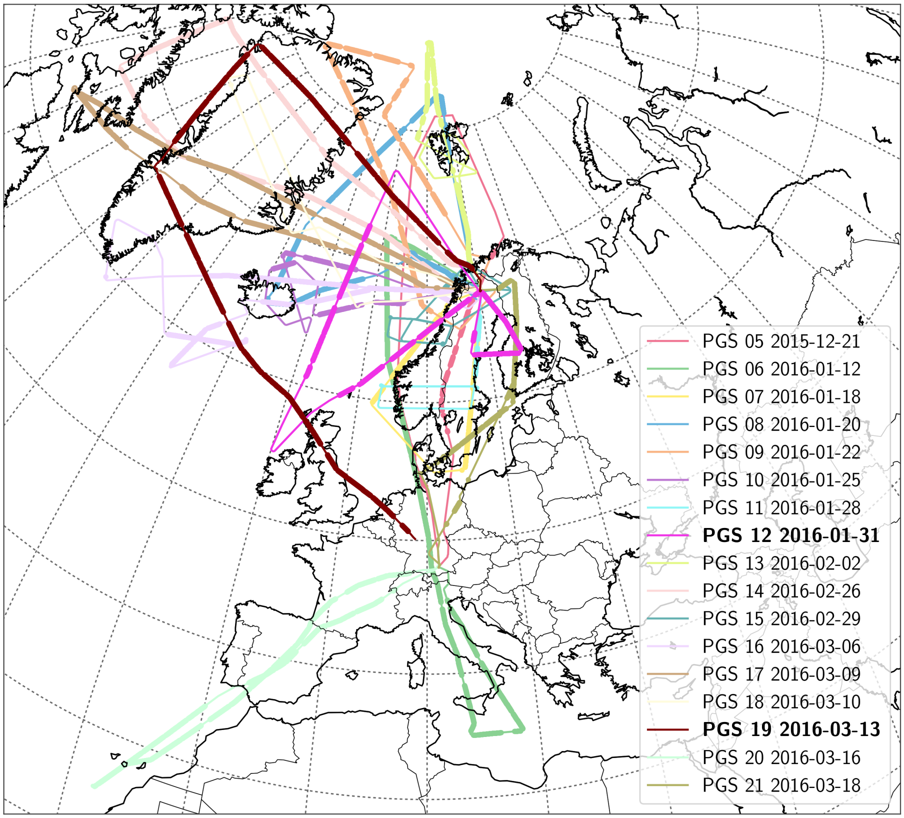

Figure 1. Flight paths of all PGS flights with GLORIA measurements. The parts of the flights with GLORIA high spectral resolution mode measurements are represented in bold lines. Flight PGS19 (13 March 2016) is discussed in detail in this paper and is highlighted in the map, together with flight PGS12, which is discussed incidentally.

aircraft and also offers the possibility to point at azimuth angles between 45° and 135° relative to the aircraft for measurements in across-track limb geometry. These different azimuth pointing angles are desired to avoid sun stray light, to correct for movements of the carrying aircraft due to cross winds or to adopt the measurement line of sight for expected horizontal gradients in temperature or trace gases. Another application of the adjustable azimuth angle is the feasibility of tomographic measurements (Ungermann et al., 2011).

The level 1 processing comprises the generation of radiometrically and spectrally calibrated spectra from raw measurement data (Kleinert et al., 2014). At first, the interferograms are corrected for spikes and for the non-linearity of the detector and readout system. Then, they are re-sampled from the time-equidistant measurement grid onto a space-equidistant grid using information of a reference laser (Brault, 1996). During re-sampling, the interferograms are corrected for possible shifts due to linear phase drifts, and the ~~off-axis angle~~ optical path difference of each pixel is ~~taken into account~~ determined according to its off-axis angle, in order to sample each interferogram onto the correct abscissa in space. After the Fourier transform, a complex calibration according to Revercomb et al. (1988) is performed. Gain and offset are determined from regular in-flight measurements of the two on-board black-bodies ~~at different temperatures. The~~ (Olschewski et al., 2013). The temperature difference between the two black-bodies is about 30 to 40 K with the cold black-body being around or slightly below ambient temperature. The spectra are apodized using the Norton-Beer "strong" apodization (Norton and Beer, 1976, 1977). This processing is done individually for each of the 48 × 128 interferograms. For noise reduction, the pixels of each detector row are averaged after filtering of bad pixels (typically 5 to 10%). As measurements are smeared along-track due to the horizontal movement of the aircraft, this averaging does not result into a loss of information. This process results in 128 row-averaged spectra with different elevation angles. After cloud filtering, this set of spectra serves as input for the retrieval of atmospheric parameters. All atmospheric parameters are retrieved from the same set of averaged spectra.

GLORIA has been deployed during the HALO campaigns TACTS/ESMVal (2012), POLSTRACC/GW-LCYCLE/SALSA (2015/2016) and WISE (2017) and during the M55 Geophysica campaigns ESSenCe (2011) and StratoClim (2016/2017). During these campaigns, the instrument has been constantly improved (Kretschmer et al., 2015), the data processing has been ~~enhanced~~ revised (Kleinert et al., 2014; Guggenmoser et al., 2015), the level 2 products have been validated (Kaufmann et al., 2015; Woiwode et al., 2015; Ungermann et al., 2015) and GLORIA data has proven to be useful for model validation (Khosrawi et al., 2017) and case studies (Rolf et al., 2015; Krisch et al., 2017). Improvements to the instrument (reduced aero-acoustic noise in the spectra) compared to the results of Woiwode et al. (2015) also increase the quality of the measured infrared spectra, resulting in different characteristics of the retrieved temperature and trace gas profiles.

2.2 In-situ instruments

On board of HALO several in-situ instruments were deployed during the PGS campaign. These in-situ instruments measure temperature and trace gases at the position of the aircraft with high precision and temporal resolution. Calibration measurements with reference gases or calibration units ~~also allow~~ assure a high accuracy of the measurements.

The AIrborne (chemical ionizaton) Mass Spectrometer (AIMS) measures HCl, SO_2, HNO_3 and $ClONO_2$ at a time resolution of 1.7 s with ~~detection limits~~ a detection limit of 6-20 pptv, and 10-15% precision~~with~~, and an accuracy of 12-20% (Jurkat et al., 2016, 2017). In addition, water vapor in low concentrations is measured in a second configuration (Kaufmann et al., 2016; Voigt et al., 2017).

Water vapor measurements between 1 and 1000 ppmv are performed with the Fast In-situ Stratospheric Hygrometer (FISH), which is based on Lyman-α photo-fragment fluorescence (Zöger et al., 1999). FISH is one of the core airborne in-situ instruments for measuring water vapor in the UTLS (Fahey et al., 2014). FISH has a time resolution of 1 s and achieved a precision of 0.7% × vmr (volume mixing ratio; relative part of the precision) + ~~/-0.35 ppmv~~ 0.35 ppmv (absolute part of the precision) with an overall accuracy of 6.6% × vmr during PGS (Meyer et al., 2015).

The Basic HALO Measurement and Data System (BAHAMAS) consists of a sensor package for basic meteorological parameters such as temperature, pressure, airflow, wind and humidity and a data acquisition system, which provides additional interfaces into the aircraft avionic system and to an inertial reference system (Krautstrunk and Giez, 2012; Giez et al., 2017). Sensor data is available with a time resolution of 100 Hz, standard processing is based on a 10 Hz time resolution. The temperature measurement is based on an open wire resistance temperature sensor, which is contained in a special Total Air Temperature

(TAT) inlet located in the nose section of the aircraft. These housings are heated to prevent ice formation and designed to separate droplets and particles from the probed airflow ahead of the sensor. The airflow is slowed down inside the housing in order to approach TAT via adiabatic heating. Data processing contains several corrections to account for deviations from ideal inlet behavior (Bange et al., 2013). These corrections limit the accuracy of the temperature determination to about 0.5 K, while the precision of the measurement is estimated to be about 0.03 K by means of ~~auto-co-variance Function~~ auto-covariance function analysis.

The ozone detector FAIRO (Fast airborne ozone instrument) was deployed on HALO with a time resolution of 10 Hz (Zahn et al., 2012). The O_3 volume mixing ratio has a precision of $\approx$0.3 ppbv (at 10 Hz) and an ~~uncertainty~~ accuracy (based on systematic errors) of $\approx$1.5%.

Additionally the Gas chromatograph for the Observation of Stratospheric Tracers Mass Spectrometer (GhOST-MS) provides measurements of CFC-12 in the electron capture detector channel (Obersteiner et al., 2016).

2.3 Aura/MLS

The NASA Earth Observing System Aura satellite was launched in July 2004 into a near-polar, sun-synchronous 705 km altitude orbit with the Microwave Limb Sounder (MLS) deployed on board. The Aura satellite flies in formation in the "A-Train" constellation of satellites and has an approximately 1:45 PM local equator crossing time. The Aura/MLS instrument is a successor to the MLS instrument on the Upper Atmosphere Research Satellite (UARS) and is a limb sounder analyzing the thermal emission (wavelengths from 2.5 to 0.1 mm) of the atmosphere using seven radiometers to cover five spectral bands (Waters et al., 2006). The ~~radiometers are pointing in the orbital flight direction and vertically~~ along track scanning radiometers scan the limb ~~in the orbit plane approximately~~ every 165 km. According to the orbit of the Aura spacecraft, the global coverage of measurements is from 82° S to 82° N. In this work, MLS version 4.2 (Livesey et al., 2017) HNO_3 and O_3 data are used. These data products have a vertical resolution of 3.0 - 4.5 km for HNO_3 and 2.5 - 3.5 km for O_3 and a horizontal resolution of 350 - 450 km and 300 - 550 km, respectively, in the UTLS. Both trace gas products have been validated for previous data versions (Santee et al., 2007; Froidevaux et al., 2008; Jiang et al., 2007).

2.4 ECMWF meteorological analysis

The input profiles for temperature, pressure and water vapor for GLORIA retrievals are taken from analysis data of the European Centre for Medium-range Weather Forecasts (ECMWF). These meteorological analyses from the "Atmospheric Model high resolution" (HRES) are available every six hours with a horizontal resolution of 1 ° and 137 vertical levels up to a top pressure level of 0.1 hPa. The global fields of temperature, pressure and potential vorticity (PV) are interpolated on a vertical grid of absolute altitude.

3 Retrieval

In order to retrieve trace gas distributions from the calibrated spectral radiances, an inverse problem has to be solved. To this end, we used the retrieval software KOPRAFIT (Höpfner, 2000), in which the forward radiative transfer is calculated by the radiative transfer model KOPRA (Karlsruhe Optimized and Precise Radiative transfer Algorithm, (Stiller, 2000)). KOPRA is a line-by-line ~~radiation transfer model~~radiative transfer model, which is optimized for computationally efficient analyses of highly resolved spectral measurements. This software is used in the processing of MIPAS-Envisat, MIPAS-Balloon and MIPAS-STR limb measurements (von Clarmann et al., 2003; Wetzel et al., 2002; Woiwode et al., 2012). KOPRAFIT employs the Jacobians (derivatives of the radiance with respect to the fitted atmospheric parameters) provided by KOPRA to fit the selected atmospheric parameters to the measured set of spectra. The inverse problem is solved by the Gauss-Newton iterative algorithm (Rodgers, 2000) with Tikhonov-Phillips regularization (Tikhonov and Arsenin, 1977; Phillips, 1962):

$$\mathbf{x}_{i+1} = \mathbf{x}_i + \left(\mathbf{K}_i^T \mathbf{S}_y^{-1} \mathbf{K}_i + \gamma \mathbf{L}^T \mathbf{L}\right)^{-1} \left(\mathbf{K}_i^T \mathbf{S}_y^{-1} (\mathbf{y} - \mathbf{f}(\mathbf{x}_i)) + \gamma \mathbf{L}^T \mathbf{L} (\mathbf{x}_a - \mathbf{x}_i)\right) \quad (1)$$

Here i denotes the iteration index, $\mathbf{x}_i$ the vector containing the atmospheric state of step i, $\mathbf{y}$ the radiance measurement vector, $\mathbf{f}$ the radiative transfer function, $\mathbf{x}_a$ the a priori profile, $\mathbf{K}_i$ the Jacobian of $\mathbf{f}$ for $\mathbf{x}_i$, $\mathbf{S}_y$ the co-variance matrix of the measurement, $\mathbf{L}$ the first order differential operator and γ the regularization parameter. The regularization term $\gamma \mathbf{L}^T \mathbf{L}$ constrains the retrieval result to a smooth profile of the retrieved atmospheric quantity. In the applied formulation, the regularization avoids a bias to the retrieval result from an ~~a-priori~~ a priori profile (Eriksson, 2000). The regularization parameters are chosen such that high vertical resolutions are obtained while unrealistic oscillations of the retrieved quantity are avoided.

The retrieval strategy in this work follows closely the one described by Woiwode et al. (2012). For the retrieval, the atmospheric parameters are represented at a discrete altitude grid with 250 m spacing in the region of interest (3 - 17 km) and coarser grid width below and above (1.5 km for 0 - 3 km, 2 km for 18 - 20 km, 2.5 km for 20 - 30 km and 50 km for 50 - 100 km). For the first step of the retrieval, trace gas profiles from the climatology by Remedios et al. (2007) are used for all important trace gases in the selected spectral range. Temperature, pressure and water vapor are taken from an interpolation of ECMWF analysis data to the GLORIA tangent points. For the water vapor retrieval, a constant profile of 10 ppmv is used as initial guess~~.~~, in order to assure independence of derived vertical and horizontal structures in the water vapor distribution e.g. compared to initial guess profiles from meteorological analysis. The retrieval quantity is either the line of sight (LOS), temperature, vmr of HNO_3, O_3, $ClONO_2$ and CFC-12 or the logarithm of vmr of H_2O. To consider atmospheric aerosols and transparent clouds, the logarithm of an artificial continuum is part of the retrieval vector as it is described in Woiwode et al. (2015).

For the preparation of the retrieval, cloud-affected spectra are filtered. For that purpose, the Cloud Index (CI) introduced by Spang et al. (2004) is calculated for each measured spectrum as the color ratio between the micro-windows 788.20 cm^{-1} to 796.25 cm^{-1} and 832.30 cm^{-1} to 834.40 cm^{-1}. The CI is shown in Fig. 2 for the flights on 31 January 2016 and on 13 March 2016. Lower CI values indicate a larger influence of clouds on the spectrum. In previous studies using comparable airborne limb emission observations, typically fixed cloud index thresholds between 2 and 4 were used (Ungermann et al., 2012; Woiwode et al., 2012, 2015). In this work, a CI threshold of 3 is used for the lowest and 1.8 for the highest limb tangent altitude to account also for observations moderately affected by PSCs. The CI thresholds for points in between are linearly

Table 1. Spectral windows for the different target species of the GLORIA high spectral resolution mode PGS retrieval

Retrieval target	Micro-window [cm^{-1}]
LOS and Temperature	810.5 - 812.9
	956.0 - 958.2
HNO_3	862.0 - 863.5
	866.1 - 867.5
	901.3 - 901.8
O_3	780.6 - 781.7
	787.0 - 787.6
$ClONO_2$	780.0 - 780.4
H_2O	795.7 - 796.1
CFC-12	918.9 - 921.3

interpolated. This approach is chosen to effectively filter out tropospheric clouds at lower altitudes while optically thin cirrus or polar stratospheric clouds still are allowed for the retrieval.

In the first step, the line of sight is determined to correct a possible misalignment of the GLORIA gimbal frame. From this retrieval a correction for the line of sight is calculated and applied to all of the following steps. Then temperature, HNO_3, O_3, CFC-12, $ClONO_2$ and H_2O are sequentially retrieved. After each step, the values retrieved for the previous quantities are kept fixed.

The spectral windows for the retrieval of the different trace gases are shown in Tab. 1. These spectral ranges were selected to minimize the cross-talk of emission lines of other trace gases, and saturation of spectral lines, particularly at low limb views, is minimized.

3.1 Error analysis

For the characterization of the results, possible error sources are estimated and their influences on the retrieval are calculated. In this work, we estimate systematic and noise errors. Considered errors are spectroscopic uncertainties (as reported in previous work), radiometric calibration errors (multiplicative gain and additive offset), residual pointing uncertainty and a temperature error for vmr retrievals~~and radiometric calibration errors, pointing uncertainty~~, and an error of the CO_2 climatology profile (accounting also for errors in the CO_2 spectroscopic line data).

The spectroscopic error is estimated as 8% for HNO_3 (Wetzel et al., 2002), 5.5% for $ClONO_2$ (Wagner and Birk, 2003) and 10% for CFC-12 (Moore et al., 2006). For O_3 and H_2O, uncertainties in line intensities are reported (Flaud et al., 2002, 2006) and the spectroscopic error is estimated as 7% for O_3 and 10% for H_2O. Considering the temperature retrieval, the spectroscopic

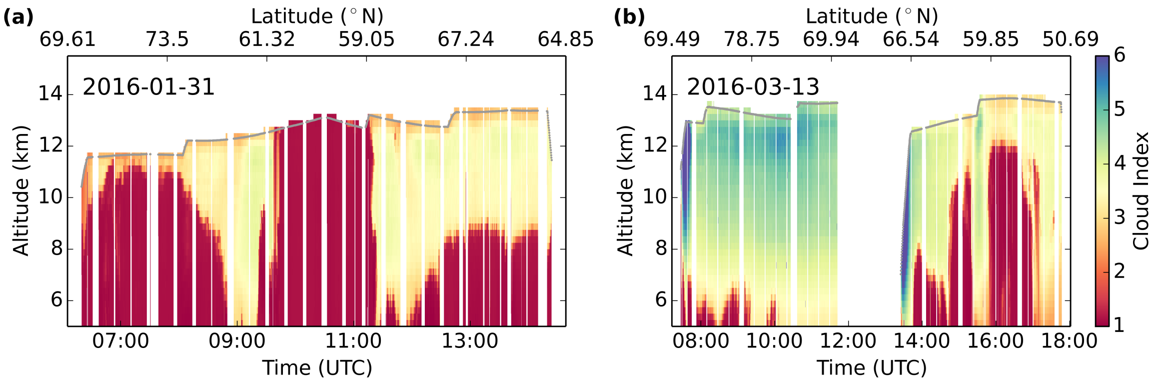

Figure 2. Vertical distribution of cloud indices along flights PGS12 (a, 31 January 2016) and PGS19 (b, 13 March 2016). The lower the cloud index, the more is the measured spectrum affected by clouds. Between 12:00 and 14:00 UTC in PGS19 no atmospheric data was measured due to a refueling stop of the aircraft.

error can be estimated by assuming an error in the CO_2 profiles as high as 5.0 %, according to Wetzel et al. (2002). In order to quantify the influence of the assumed CO_2 profile, the temperature retrieval has been repeated with a CO_2 profile uniformly decreased by 5%. The differences between these retrievals at each grid point show the sensitivity of the retrieval to the modified CO_2 profile.

In the same way the impacts of further error sources on the retrieval are quantified~~:~~. The results of a retrieval with a perturbed radiometric calibration, LOS or temperature are subtracted from the standard retrieval to estimate the error of each individual retrieval grid point. With this method, uncertainties in the radiometric calibration ~~, which can be attributed to errors in the multiplicative gain and the additive radiance offset,~~ are calculated considering uncertainties in ~~multiplicative gain enhancement~~ the multiplicative gain of 2% and ~~an additive~~ uncertainties in the additive radiance offset of 50.0 nWcm^{-2}sr^{-1}cm~~radiance offset~~. LOS errors are estimated by retrievals ~~involving~~ assuming a 0.05° LOS offset~~considering the~~. This estimation is based on the short-term profile-to-profile variability found in the LOS ~~retrieval~~ retrievals (see Sec. 4.3.1), and systematic uncertainties inherent to the LOS retrieval, such as uncertainties in ECMWF atmospheric temperature and pressure. For trace gas retrievals, the retrieved temperature is used to describe the atmospheric state. The effect of uncertainties in the retrieved temperatures on the trace gas retrievals is estimated by modifying the retrieved temperature profile systematically with the related temperature error (estimated for the temperature retrieval). The retrieval noise is calculated according to Rodgers (2000)

$$\Delta x_{\text{noise}} = \mathbf{G}_y \epsilon = \left(\left(\mathbf{K}^T \mathbf{S}_y^{-1} \mathbf{K} + \gamma \mathbf{L}^T \mathbf{L} \right)^{-1} \mathbf{K}^T \mathbf{S}_y^{-1} \right) \cdot \epsilon \, . \qquad (2)$$

Here, Δx_{noise} denotes the noise error, $\mathbf{G}_y$ the retrieval gain matrix, ϵ the measurement error and $\mathbf{K}$ the Jacobian for the last iteration step. This measurement error is estimated as the spectral variance in the micro-window of the imaginary part of the calibrated spectrum (Kleinert et al., 2014).

The total estimated error for each altitude of each retrieved profile is calculated as the square root of the sum of the squares of each error contribution, as is shown for vmr in Eq. (3) and for temperature in Eq. (4).

$$\Delta x_{\text{vmr}} = \sqrt{\Delta x^2_{\text{spectroscopy}} + \Delta x^2_{\text{gain}} + \Delta x^2_{\text{offset}} + \Delta x^2_{\text{pointing}} + \Delta x^2_{\text{temperature}} + \Delta x^2_{\text{noise}}} \quad (3)$$

$$\Delta x_{\text{temperature}} = \sqrt{\Delta x^2_{\text{CO}_2} + \Delta x^2_{\text{gain}} + \Delta x^2_{\text{offset}} + \Delta x^2_{\text{pointing}} + \Delta x^2_{\text{noise}}} \quad (4)$$

3.2 Vertical resolution and degrees of freedom

An important diagnostic measure is the vertical resolution, which is calculated by using the averaging kernel of the retrieval. The averaging kernel matrix is defined as (Rodgers, 2000)

$$\mathbf{A} = \mathbf{G}_y \cdot \mathbf{K}\,. \quad (5)$$

The vertical resolution at a retrieval grid point is calculated as the full width at half maximum of the averaging kernel row. Another important quantity for a retrieval is the number of degrees of freedom. These are calculated as the trace of the averaging kernel matrix (Rodgers, 2000), since the diagonal ~~element of each averaging kernel row is a measure~~ elements of the averaging kernel are measures of how much measurement information is contained in the retrieval result per level.

4 Results

The results of the GLORIA measurements for the flight on 13 March 2016 (PGS19) are shown in the following part. Flight PGS19 is selected as an example of continuous measurements in high spectral resolution mode, and as an example of an illustrative amount of atmospheric variability within the measured air masses. Results for all of the other 14 PGS research flights with GLORIA measurements in high spectral resolution are shown in the ~~appendix~~supplement. First, the meteorological and chemical background situation of this flight day and region is discussed on the basis of MLS measurements at a level corresponding with a typical flight altitude for this specific flight. Then one example temperature and HNO_3 profile is characterized in detail. The main part of this section is the discussion of the GLORIA retrieval results for flight PGS19. For the discussion of the elevation angle correction also results for the flight on 31 January 2016 (PGS12) are shown as an example for a different type of LOS distortion and correction. In order to provide a survey of all GLORIA measurements and their quality during the whole PGS campaign, comparisons to in-situ and MLS measurements are presented as an overview.

4.1 Meteorological situation for flight PGS19 on 13 March 2016

The flight PGS19 on 13 March 2016 was the transfer back from the campaign base in Kiruna, Sweden to Oberpfaffenhofen, Germany. This flight was planned to sample aged vortex air over the northwestern part of Greenland and to cross a region of subtropical air associated with a high tropopause between the East coast of Greenland and Ireland. Take-off in Kiruna was at 07:08 UTC and touch-down in Oberpfaffenhofen at 18:28 UTC. The first part of the flight was directed towards the north-western coast of Greenland (see Fig. 3 way point "A"), flying over the Norwegian sea and then in a southern direction to a refueling stop at Kangerlussuaq airport in Greenland (way point "B"). ~~This stop allowed for higher altitudes of the HALO~~

~~aircraft before refueling due to lower aircraft weight. Otherwise, the necessary altitude~~ HALO reaches its peak ceiling altitude immediately before each refueling stop, when the air frame is at its lightest. At these phases of the flight, the flight altitude is high enough to sample subsided polar air masses over the northern part of Greenland could not have been reached. After this stop, the aircraft passed the northern Atlantic ocean and the British Isles towards Oberpfaffenhofen in southern Germany.

The meteorological situation during this flight is shown in Fig. 3 (top row) with temperature (a) and potential vorticity (PV, b) at a level corresponding to a typical flight altitude of 13 km for this specific flight. At this altitude and time of the winter, the PV determining the edge of the polar vortex according to Nash et al. (1996) is estimated as ≈ 9 PVU. The first part of the flight (until way point "A") took place in relatively warm 220 to 230 K air masses compared to the rest of the flight. PV increased along the flight track towards maximum values of more than 12 PVU. This indicates that the flight entered the late winter polar stratosphere and presumably even aged subsided polar vortex air. During the flight leg between the way points "A" and "B", the aircraft remained within these stratospheric air masses with relatively warm temperatures and high PV. On the flight leg from way point "B" towards the final destination Oberpfaffenhofen, HALO ~~departed~~ left these air masses, with temperatures decreasing ~~down~~ to 200 K and PV down to 4 PVU over the northern Atlantic ocean. The air masses above the British Isles and central Europe showed temperatures of up to 210 K and PV of 6 to 9 PVU with fine filaments visible on the PV map. This might point to air masses remaining from the dissolving late winter polar vortex.

For a comparison of the MLS measurements with GLORIA, the MLS data has been selected for ~~days of and time periods around~~ dates and times of PGS flights, filtered ~~regarding~~ by data quality as recommended by Livesey et al. (2017) and interpolated onto a regular horizontal grid (2° latitude × 4° longitude) using a squared cosine as the weighting function. The width of this squared cosine function has been chosen to be 1.5° for latitudes and 8.0° for longitudes, and a minimum threshold of 0.75 is selected. Additionally, the pressure coordinate of the MLS data is interpolated to geometric altitude for an easier comparison to the GLORIA data. This interpolation method does not provide meaningful comparisons of water vapor because tropospheric H_2O (in contrast to stratospheric HNO_3 and O_3) is likely to ~~significantly change~~ vary significantly within the time range of Aura/MLS measured profiles, which are selected for this type of interpolation. For this reason~~no comparisons~~, no comparison of GLORIA and Aura/MLS H_2O measurements ~~are~~ is shown.

An overview of these gridded MLS HNO_3 and O_3 horizontal distributions is shown in Fig. 3 (bottom row) at a typical flight altitude of 13.0 km for PGS flight 19 on 13 March 2016. The HALO flight track and geolocations (position and altitude) of GLORIA tangent points are also shown on these maps. Along the flight track, local minima in MLS HNO_3 are observed above the Norwegian sea and south of Iceland. Local maxima in MLS HNO_3 and O_3 are present above the northern part of Greenland at way point "A".

4.2 Characterization of example profiles

The quality of the retrieved GLORIA data can be assessed by the estimated errors (see Sect. 3.1) and by the vertical resolution (see Sect. 3.2). These quantities are shown in Fig. 4 as an example for the retrieval result of a temperature and nitric acid profile. In the left column (a,d) of this figure the retrieval results and the initial guess profiles are shown; the right panel (c,f) shows the vertical resolution. For these retrievals vertical resolutions of 400 m to 750 m are achieved. It can be seen that the

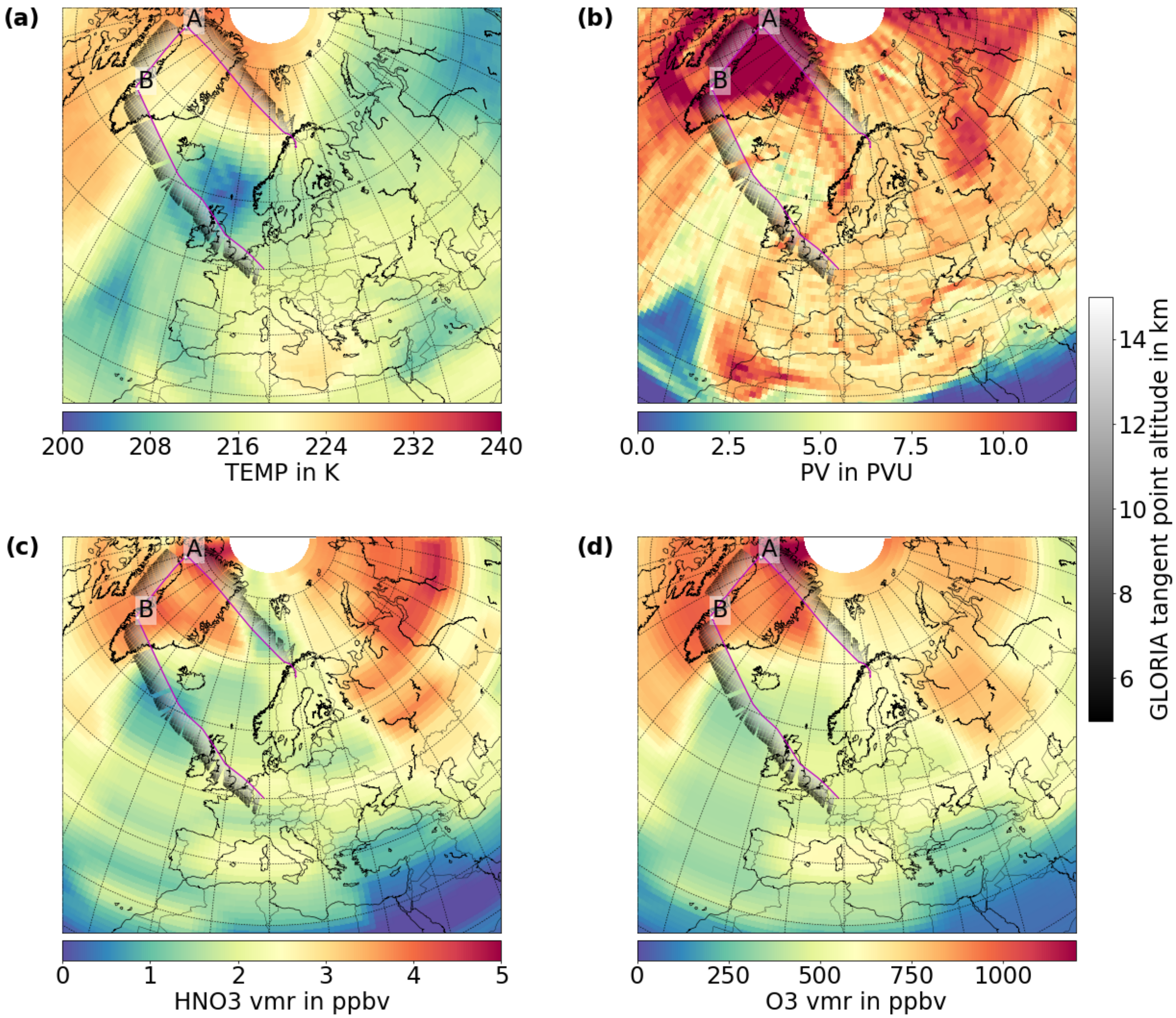

Figure 3. (a) Temperature and (b) potential vorticity (PV) from ECMWF meteorological analysis on 13 March 2016 12:00 UTC at 13.0 km and (c) MLS HNO_3 and (d) O_3 measurements on 13 March 2016 between 6:00 and 18:00 UTC (approximation for the time period of flight PGS19) interpolated to a regular latitude/longitude grid and typical HALO cruising altitude of 13.0 km. For flight PGS19 on this day, the ground track of the HALO aircraft is shown with a magenta line and the geolocations of GLORIA tangent points are shown along the flight track with points in the greyscale color map. Way points of this flight are marked with capital letters.

shapes of the retrieved temperature and vmr profiles ~~and their shapes significantly differ~~ differ significantly from the initial guess profiles at an altitude range between 5.5 km and 13.5 km, reflecting the weak influence by the Tikhonov regularization. Below these altitude ranges the profile shapes resemble those of the initial guess profile and no information is contributed by the measurement. Above 13.5 km, the retrieved profiles are also influenced by measurements with upward looking lines of sight, which explains the small differences in shape at these altitudes. In this region the vertical resolution is poor and thus little measurement information is obtained for these parts of the profiles.

In the second column (b,e) of Fig. 4, individual 1σ error contributions are shown. For the temperature the total estimated error is ~~most~~ predominantly influenced by radiometric gain calibration (up to 1.0 K) and pointing uncertainties (in the range of 0.5 to 1.5 K). In the case of HNO_3, the total estimated error is dominated by the spectroscopy error estimated as a constant relative fraction of 8.0 % (as assumed in Sec. 3.1) and the uncertainties due to the previously retrieved temperature data (up to 0.3 ppbv). The pointing error has large contributions (up to 0.6 ppbv) to the total estimated error at altitude ranges where large vertical gradients in the profiles occur. At these altitude ranges with large vertical gradients even small changes in the elevation pointing have large influence on the absolute differences between the perturbed and the reference retrieval result. The radiometric offset and the retrieval noise error only contribute a minor part of the total error ($\leq$0.5 K for temperature and up to $\leq$0.2 ppbv for HNO_3).

In the following discussion of the results, the retrieved profile, vertical resolution, total estimated error are presented as curtain plots for a whole research flight. This ~~shall provide an overview of~~ simultaneously illustrates the amount of data that has been measured by GLORIA~~and still allow~~, and allows the characteristics of the results to be shown in detail.

4.3 GLORIA results

4.3.1 Line of sight

For each flight, one systematic pointing correction is derived from the retrieval. The pointing elevation angle is retrieved to compensate for systematic misalignment of the pointing system of GLORIA. The LOS retrieval results for the flights on 31 January 2016 and on 13 March 2016 are shown as the difference between expected and retrieved elevation angle (black dots in Fig. 5). This difference in the retrieved LOS can be caused by ~~changes of~~ differences in the atmospheric state compared to the ECMWF fields ~~,~~ (which also affects the intensity of the CO_2 spectral lines, that are used for the LOS retrieval), thermal deformation of the instrument, and a systematic error of the pointing calibration on ground. Fluctuations in the retrieved LOS are attributed to the changes of the atmospheric state not resolved or reproduced by the ECMWF fields and the thermal deformation, while the systematic error of the calibration is expected to result in a time-independent LOS offset. With the diagnostic data available, it is not possible to distinguish between atmospheric variations and thermal deformations of the instrument. Ground-based measurements suggest that the thermal deformations of the instrument are an important cause for these variations, but also the atmospheric variation of temperature and pressure is estimated to have a major impact. For that reason generally, only one average LOS correction value per flight is used. For future campaigns it is planned to ensure the quality of the pointing by ground-based absolute pointing calibrations and by in-flight measurements of the moon on a regular basis. An example of this average correction, which is applied for flights between 02 February 2016 and 18 March 2016, is shown in Fig. 5 (b, ~~blue~~ red points).

For flights between 21 December 2015 and 31 January 2016 a software malfunction of the pointing control software caused the LOS to drift away from the commanded elevation. At certain points the software changed the instrument elevation back to its

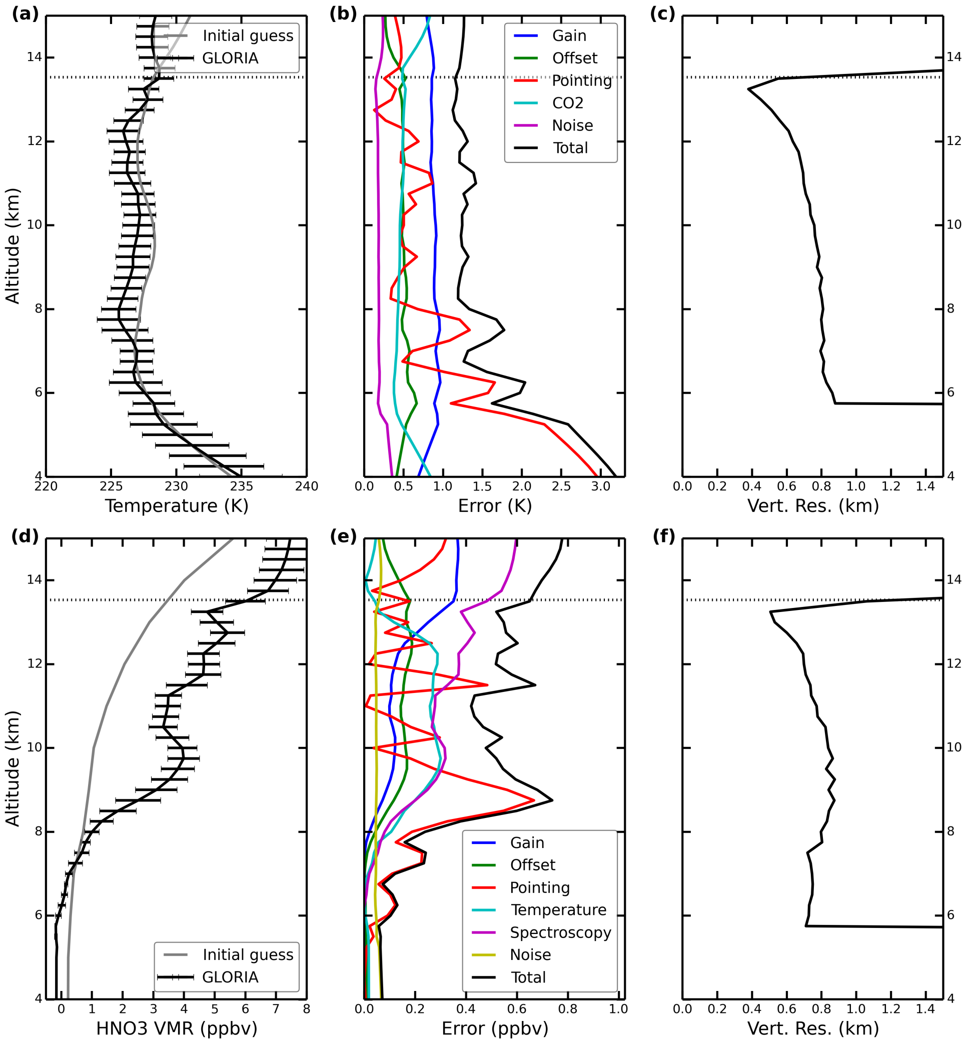

Figure 4. Illustration of the error budget of the temperature and HNO_3 retrieval of Flight 19 on 13 March 2016 for a selected profile at 10:37:06 UTC. First column: retrieved vertical profile of temperature (first row) and HNO_3 (second row) with total estimated error (black) and initial guess profile (grey). The retrieved profile has 14.9 and 12.5 degrees of freedom for temperature and HNO_3, respectively. Second column: Different total error contributions and estimated total error. Last column: Vertical resolution of this retrieval result. The dotted line represents the flight altitude of the aircraft.

correct value and steep steps in the retrieved pointing elevation angle are observed in these flights (see Fig. 5 a, enlargement: "Drift" and "Jump"). A correction of this artifact can be calculated by interpolating the LOS between the points immediately after a steep step. This interpolated line between the correct elevation angles approximates the LOS that would have been retrieved for a measurement without this software malfunction. The same average LOS correction, which is used for other

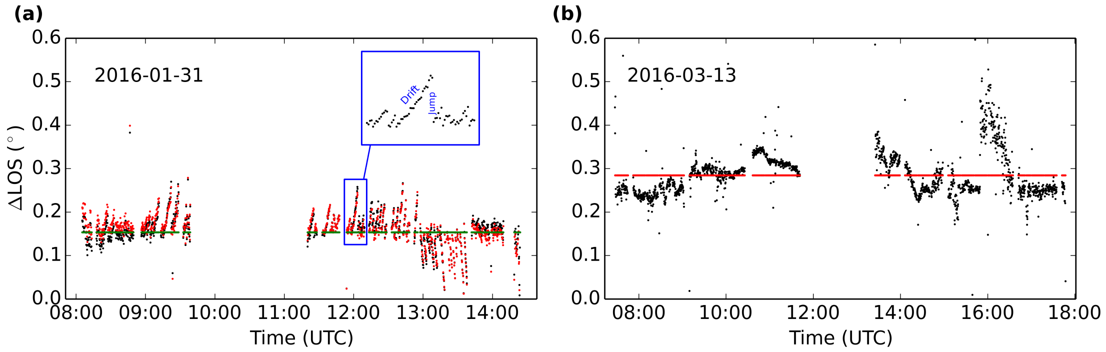

Figure 5. Line of sight correction of two flights (a: PGS12, b: PGS19) during the PGS campaign. The retrieved deviation of the LOS from the nominally set value is shown in black, the applied correction in ~~blue~~ red and for flight PGS12 the averaged LOS (before applying the correction of the drift) in green.

flights, can be calculated from this interpolated LOS (Fig. 5 a, green points). ~~The~~ This is the first part of the LOS correction for these flights. In the second part, the influence of the software malfunction can be extracted by subtraction of the interpolated LOS from the retrieved LOS. For an idealized measurement (without any further error in the LOS), this method separates the effect of the software malfunction from long-term variations (which have been corrected for in the first part). For subsequent retrievals of temperature and volume mixing ratios, both corrections, the average LOS correction and the correction of the steps, have been applied (Fig. 5 a, ~~blue~~ red points).

4.3.2 Temperature

The retrieved temperature along with characterization diagnostics and comparison to in-situ observations for the flight PGS19 is shown in Fig. 6. The retrieval result in the panel (a) shows the temperature profiles in a color coded curtain plot. This type of plot is also used to present the curtains of volume mixing ratio results. The lower horizontal axis indicates the measurement time and the upper horizontal axis the corresponding latitude of the aircraft. The vertical axis shows the absolute altitude of the retrieval grid points. The retrieval result is filtered according to the vertical resolution. Only data points with a vertical resolution better than 2 km are presented. For that reason, the data above flight level is filtered out. Also the measured spectra below cloud tops have been filtered out prior to the retrieval. The time between 12:00 and 13:00 UTC was spent on the ground due to a refueling stop of the aircraft. Smaller gaps between the profiles are due to radiometric calibration measurements. As a measure for the dynamical tropopause, the ECMWF potential vorticity interpolated to the GLORIA tangent points is shown in magenta dashed lines, marking the values of 2.0 and 4.0 PVU. In the first part of the flight (until way point "B"), high temperatures are observed. The dynamical tropopause is at low altitudes down to 6 km, and mainly stratospheric air masses are sampled by GLORIA during this part of the flight. These stratospheric air masses at low altitudes suggest subsidence of air

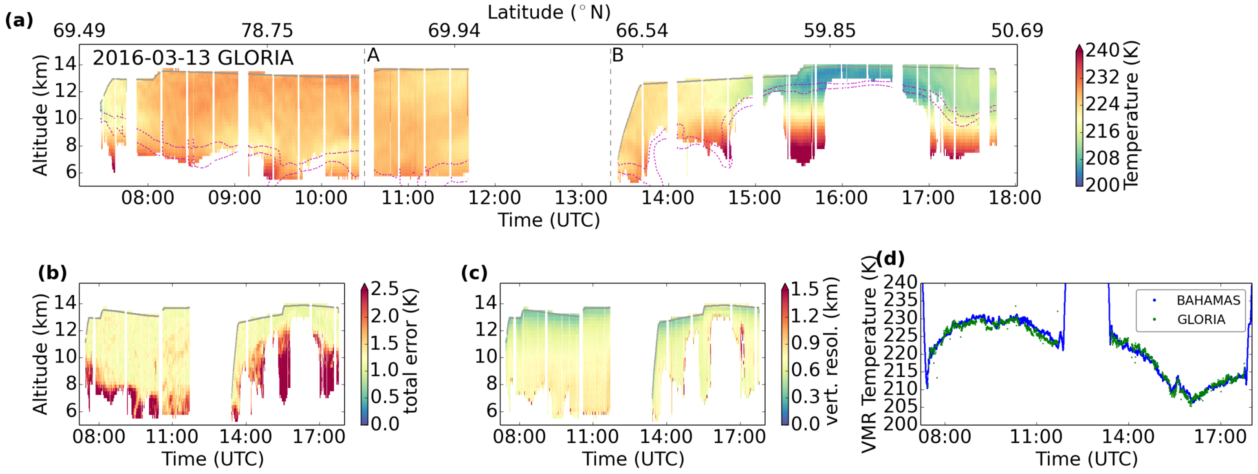

Figure 6. Temperature flight PGS19: Cross section of (a) retrieved temperature (the flight altitude is marked with a grey line; white spaces mark regions without data, the ECMWF potential vorticities of 2 and 4 PVU are marked with magenta dashed lines, way points are marked with grey vertical dashed lines) and cross sections of (b) estimated total error and (c) vertical resolution, followed by (d) comparison of the GLORIA measurements (green) to the BAHAMAS in-situ measurement (blue).

masses from the polar vortex during the late winter. The second part of this flight shows the transition to a higher tropopause up to 12 km and also stronger vertical gradients from higher temperatures (240 K) at lower altitudes~~to lower temperatures down to~~, down to temperatures as low as 205 K at flight altitude. The last hour of measurements shows again a lower tropopause and less steep vertical gradients.

The total estimated error (b) indicates for most data points values in the range of 1.0 to 1.3 K. Especially at regions with higher temperature, the retrieval results are less accurate due to higher gain error contributions. The main error contribution is the pointing error due to vertical gradients. The vertical resolution (c) of the temperature retrieval is between 500 m and 800 m. Altitudes closer to the aircraft usually show a better vertical resolution due to denser spacing of the tangent points.

In-situ measurements taken at flight level are compared to the GLORIA retrieval results obtained close to the flight altitude. From each vertical profile retrieved from GLORIA the grid point, which is closest to the flight altitude (i.e. between 0 and 250 m underneath the flight altitude) and which has a vertical resolution better than 2 km, is chosen for comparison. This assures the best possible match of sampled air masses with the in-situ instrument. It is important to keep in mind, that the data sets do not probe exactly the same air-masses, since GLORIA measures at the limb and thus collects the radiation from a long path of ≈ 100 km through the atmosphere (Ungermann et al., 2012, 2011). In Fig. 6(d) the comparison of GLORIA temperatures (green dots) to the BAHAMAS in-situ measurements (blue dots) is presented. The two measurements show agreement to within 1.3 K, which is the estimated error of the GLORIA temperature retrieval.

4.3.3 Nitric acid

Due to the formation and sedimentation of polar stratospheric clouds and the resulting de- or re-nitrification (Peter and Grooß, 2011), nitric acid (HNO_3) is expected to display irregular small structures in the UTLS region. For that reason, it is important to achieve spatially highly resolved and validated measurements of HNO_3 in the UTLS. The GLORIA retrieval results for the flight PGS19 are presented in Fig. 7. The two-dimensional distribution of HNO_3 volume mixing ratios shows fine structures with maximum values up to 7 ppbv. The retrieval has a typical vertical resolution of 500 to 800 m, and the error is typically 0.5 ppbv. The comparison to the in-situ measurements by AIMS is given in Fig. 7(e). The strong fluctuations of HNO_3 are captured simultaneously by both instruments. The agreement between the instruments is often better than 0.5 ppbv. However, at some locations their differences reach up to 2.0 ppbv. These discrepancies reflect the large atmospheric variability ~~likewise~~ in the horizontal direction due to ~~de-/nitrification~~ de-nitrification processes along the GLORIA line of sight. The horizontal distribution of PV (Fig. 3(b)) suggests that at this part of the flight (from way point "B" to the final destination Oberpfaffenhofen) air masses influenced by outflow of the polar vortex are sampled, which explains higher variability in trace gas distributions. This atmospheric variability is also ~~implied~~ visible in the MLS HNO_3 horizontal distribution along the GLORIA viewing direction as shown in Fig. 3(c). For a qualitative comparison to the GLORIA measurements, the gridded MLS HNO_3 data has been interpolated to the GLORIA tangent points (Fig. 7(b)). Considering the different spatial resolutions of the GLORIA and the MLS data, both HNO_3 distributions show relative minima and maxima at the same locations and the absolute values are of the same order of magnitude. Due to the lower vertical resolution of MLS HNO_3 measurements, they are more influenced by air masses at higher altitudes and small structures cannot be resolved. This difference in spatial resolution explains lower absolute HNO_3 in MLS compared to GLORIA. The advantage of the satellite product, though, is information about air masses above the HALO flight altitude and how these large scale structures of HNO_3 are connected with the filaments measured by GLORIA.

4.3.4 Ozone

The measured ozone (O_3) distribution during the flight PGS19 can be found in Fig. 8, where maximum values up to 1600 ppbv at altitudes of 13 km are observed. Below this maximum, finer structures are present. Spatial features are in agreement with the ones observed in HNO_3 (see Fig. 7), which is expected from atmospheric chemistry (Popp et al., 2009). This close correlation between the GLORIA measurements of both trace gases is an additional self-check for the validity of our results. The total estimated error (up to 150 ppbv) is dominated by spectroscopic and gain uncertainties. Vertical resolutions from 500 to 900 m are achieved. In comparison to the FAIRO in-situ measurements, the GLORIA retrieval results follow the long-term as well as the short-term variations. The agreement of the two measurements is typically better than 100 ppbv. In regions of maximum observed O_3 mixing ratios high profile-to-profile variations up to 200 ppbv are visible. These variations are explained by the estimated total error and by the expected atmospheric variability along the GLORIA line of sight. In the second part of the flight, GLORIA and FAIRO ozone data show different structures and differences between the measurements up to 300 ppbv. This is the same region, where the HNO_3 in-situ comparison shows differences and where an inhomogeneous horizontal distribution is suspected to distort the comparison of these measurements. The horizontal distribution of O_3 at 13 km altitude as

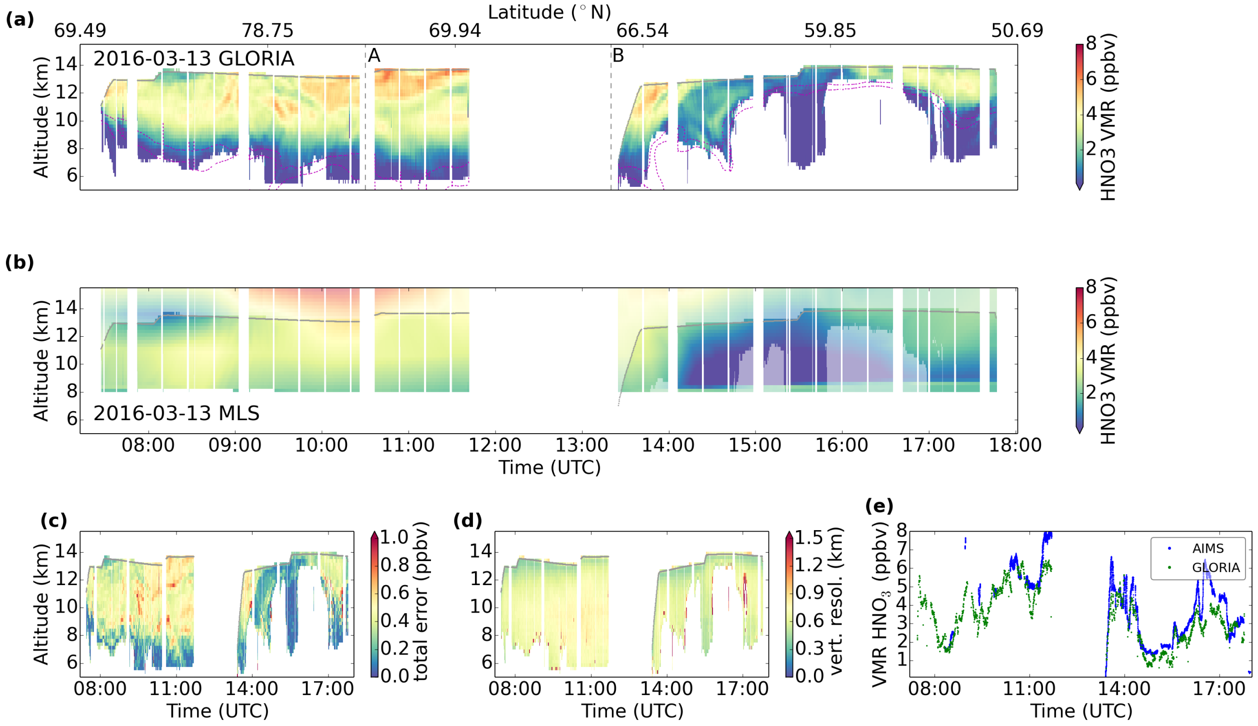

Figure 7. HNO_3 flight PGS19: Cross section of (a) retrieved HNO_3 volume mixing ratio (the flight altitude is marked with a grey line, the ECMWF potential vorticities of 2 and 4 PVU are marked with magenta dashed lines, way points are marked with grey vertical dashed lines). Cross section of (b) MLS HNO_3 data interpolated to the GLORIA tangent points and above the aircraft. Regions with no corresponding GLORIA measurement are marked by fainter colors. Cross sections of (c) total estimated error, (d) vertical resolution and (e) comparison of the GLORIA measurements (green) to the AIMS in-situ measurement (blue)

derived from MLS measurements is illustrated in Fig. 3d. A horizontal gradient is seen above Baffin Bay (the region covered by the GLORIA tangent points between way points "A" and "B"; higher O_3 volume mixing ratios in the GLORIA line of sight compared to the aircraft position). The comparison of GLORIA O_3 to the MLS distributions interpolated to the GLORIA geolocations shows very similar large-scale structures in both data sets. Again, small scale structures which are visible in GLORIA measurements are not captured in the lower resolution MLS data.

4.3.5 Chlorine nitrate

Chlorine nitrate ($ClONO_2$) is one of the two reservoir species (the other being HCl) of chlorine in the stratosphere. As was initially shown by infrared limb emission observations (Clarmann et al., 1993; Oelhaf et al., 1994; Roche et al., 1994), chlorine deactivation in the Arctic spring region results in strong enhancement of $ClONO_2$. The retrieved $ClONO_2$ distribution in Fig. 9 shows several fine structures and maximum values up to 1500 pptv in the flight section (way points "A" to "B") that reached

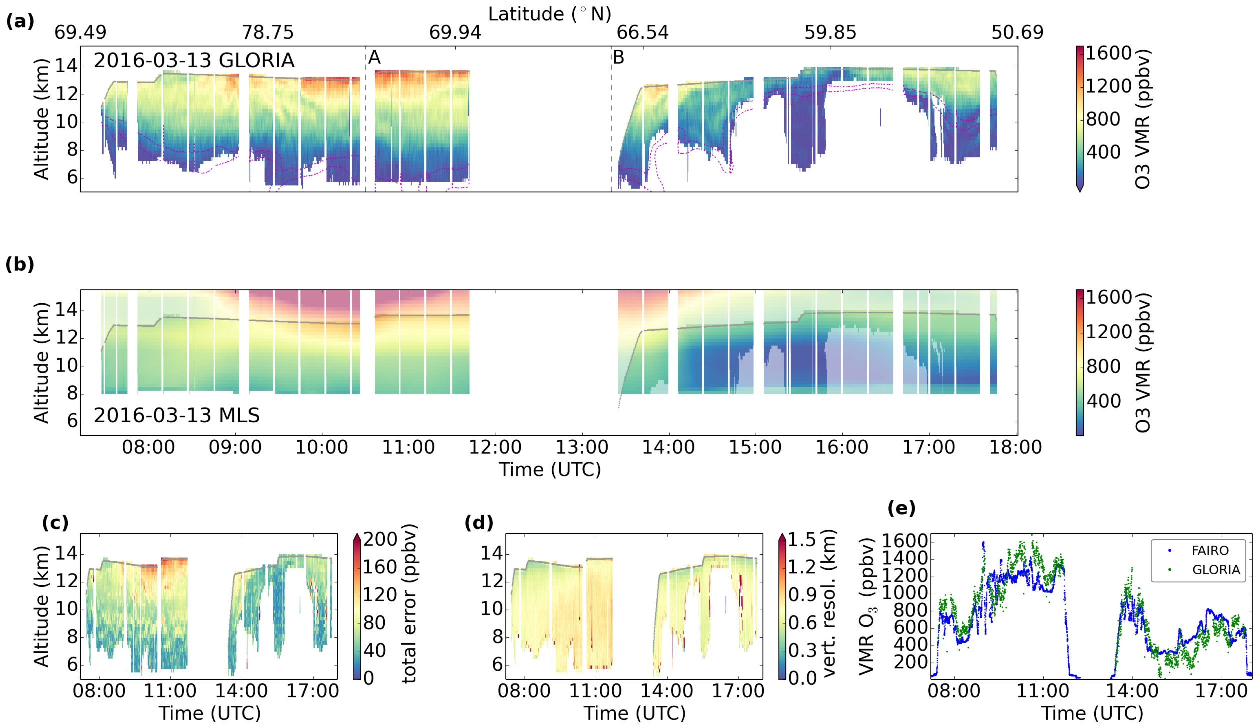

Figure 8. O_3 flight PGS19: Cross section of (a) retrieved O_3 volume mixing ratio (the flight altitude is marked with a grey line, the ECMWF potential vorticities of 2 and 4 PVU are marked with magenta dashed lines, way points are marked with grey vertical dashed lines). Cross section of (b) MLS O_3 data interpolated to the GLORIA tangent points and above the aircraft. Regions with no corresponding GLORIA measurement are marked by fainter colors. Cross sections of (c) total estimated error, (d) vertical resolution and (e) comparison of the GLORIA measurements (green) to the FAIRO in-situ measurement (blue).

the highest PV values (see Fig. 3(b)), which can be interpreted as subsided deactivated chlorine in form of $ClONO_2$. The corresponding values of total estimated error are 150 pptv. In case of background values (< 100 pptv), the estimated errors are 30 pptv. The increased errors for enhanced values are caused by the impact of relatively increased gain errors. Vertical resolutions of 500 m to 900 m are calculated for this retrieval. The comparison to the AIMS in-situ measurements of $ClONO_2$ shows agreement of the two data products to within 200 pptv, except for the maximum values, where differences are up to 500 pptv. Here, the GLORIA retrieval shows a lower absolute vmr but a similar structure. Again, we attribute this difference to an offset in altitude and a possible horizontal gradient, which is measured as an average along the GLORIA line of sight.

4.3.6 Water vapor

Water vapor (H_2O) is mainly present in the troposphere. GLORIA H_2O distributions are interesting for investigations of mesoscale structures such as tropopause folds (Shapiro, 1980). In polar studies, H_2O is of interest because these distributions

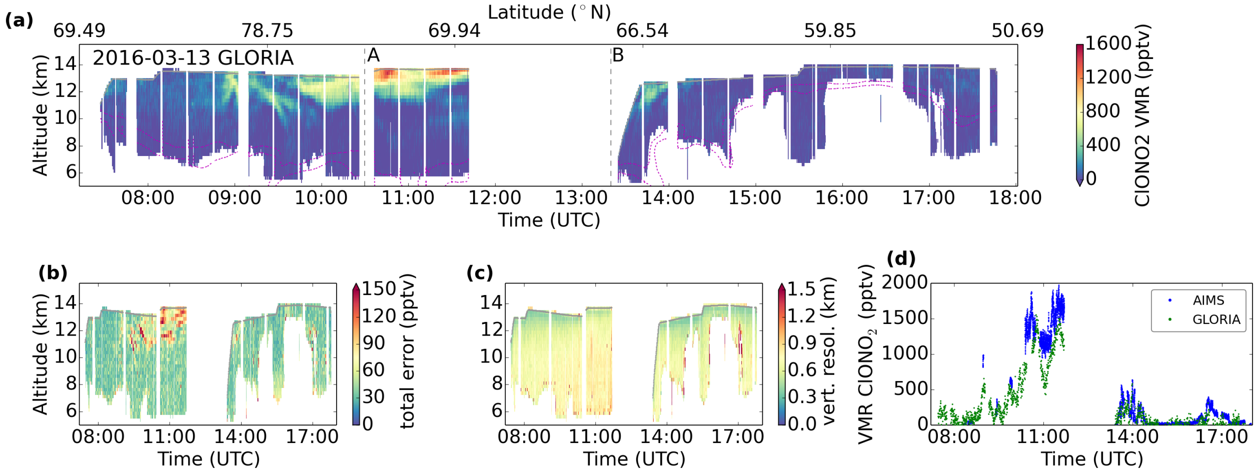

Figure 9. $ClONO_2$ flight PGS19: Cross section of (a) retrieved $ClONO_2$ volume mixing ratio (the flight altitude is marked with a grey line, the ECMWF potential vorticities of 2 and 4 PVU are marked with magenta dashed lines, way points are marked with grey vertical dashed lines). (b) Cross sections of total estimated error, (c) vertical resolution and (d) in-situ comparison of the GLORIA measurements (green) to the AIMS in-situ measurement (blue).

are used to understand the formation and decay of polar stratospheric ice clouds (de-/hydration) (Fahey et al., 1990). The distribution of H_2O reflects the tropopause altitude with very low ~~stratopsheric~~ stratospheric values ($\approx$ 5 ppmv) in the region of the aged vortex (way points "A" to "B") and high values (10-20 ppmv) above the intrusion of subtropical air where HALO was close to the tropopause (way point "B" to the final destination Oberpfaffenhofen). The total estimated error shows higher values (> 5 ppmv) in regions with enhanced H_2O vmr compared to errors lower than 1 ppmv in regions with measured stratospheric background values. The vertical resolution is between 400 m and 700 m. The comparison to the FISH in-situ measurement shows agreement to within the GLORIA error of typically 1 ppmv. The enhancement at flight altitude at 15:30 UTC is well captured in both data sets.

4.3.7 Chlorofluorocarbon 12

Dichlorodifluoromethane (CFC-12) is a chlorofluorocarbon that has been artificially produced for usage as refrigerants and aerosols. Its production is regulated by the Montreal Protocol due to its potential for ozone depletion (WMO, 2015). Because of its vertical gradient, CFC-12 can be used as a tracer for tropospheric air and for the altitude of the air masses (Greenblatt et al., 2002). The vmr distribution along flight PGS19 of CFC-12 is presented in Fig. 11. Here, mainly volume mixing ratios of about 500 pptv are observed in the troposphere. In the area where aged subsided vortex air was reached (way points "A" to "B"), values as low as 320 pptv were found. The error is between 40 and 130 pptv. The vertical resolution is in the range of 500 m to 1000 m. The comparison to the in-situ measurements by GhOST-MS shows agreement to within 70 pptv. The high profile-to-profile variation up to 100 pptv of GLORIA CFC-12 that can be seen in this in-situ comparison plot exceeds the total

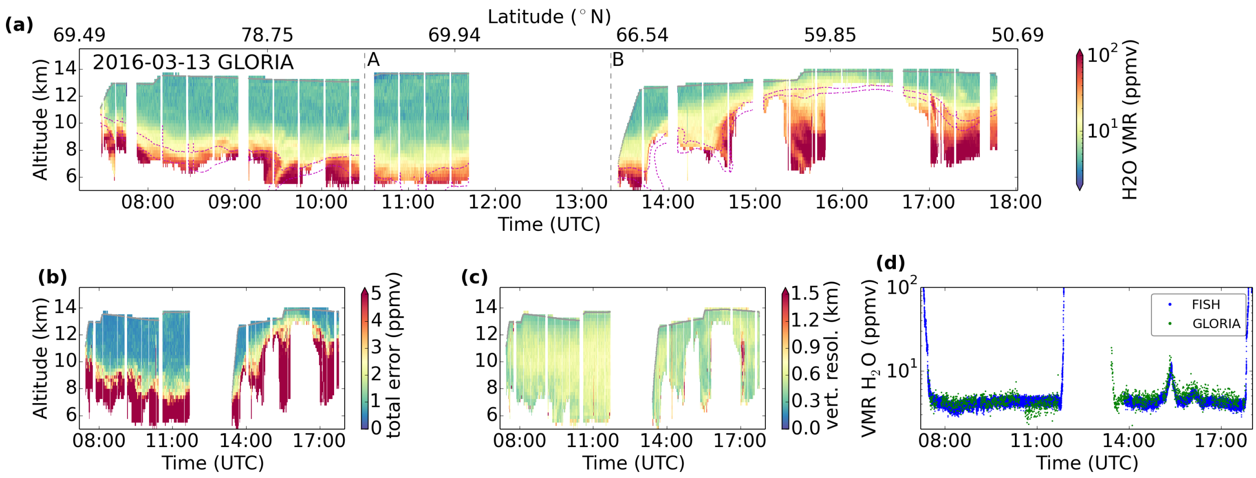

Figure 10. H_2O flight PGS19: Cross section of (a) retrieved H_2O volume mixing ratio (the flight altitude is marked with a grey line, the ECMWF potential vorticities of 2 and 4 PVU are marked with magenta dashed lines, way points are marked with grey vertical dashed lines). Cross sections of (b) total estimated error,(c) vertical resolution and (d) comparison of the GLORIA measurements (green) to the FISH in-situ measurement (blue).

estimated error at flight altitude of ≈70 pptv. So it is likely, that atmospheric variability along the GLORIA line of sight might cause these fluctuations. This variability is also present in all other flights of this campaign (see Tab.2). Also, compared to other GLORIA retrievals, a higher number of extreme outlier points are observed in the GLORIA data. This is an indication that the retrieval for CFC-12 is more sensitive to perturbations in the spectra (e.g. high altitude clouds that have not been effectively filtered) compared to the retrievals of temperature and other trace gases.

4.4 Overview of in-situ comparisons for the PGS campaign

For an overview of comparisons of GLORIA high spectral resolution retrieval results to in-situ measurements for all PGS flights, the median difference and the median absolute deviation (Rousseeuw and Croux, 1993) are presented in Tab. 2. The median difference gives a measure of the accuracy of the match between the data sets, and the median absolute deviation is a method for describing the spread around this median value. Both measures are robust methods and for that reason a few extreme mismatches do not have a large influence. Detailed plots for flights that are not described as thoroughly as the flight PGS19 are provided as a supplement. Those plots also help to understand larger deviations (e.g. in temperature) between GLORIA and in-situ measurements that are present in numerous flights in January 2016, which have been strongly affected by PSCs at and above flight level. ~~The~~ From the HALO flight crew, PSCs have been reported at these altitudes for PGS flights until PGS14 (26 February 2016). The influence of PSC and high altitude cirrus clouds on the spectra are shown in Fig. 2a as lower CI values at and below flight altitude. The comparisons of GLORIA and in-situ instruments over the whole campaign show that there are reasonably low biases between the data sets. Atmospheric conditions that influence the measurement conditions

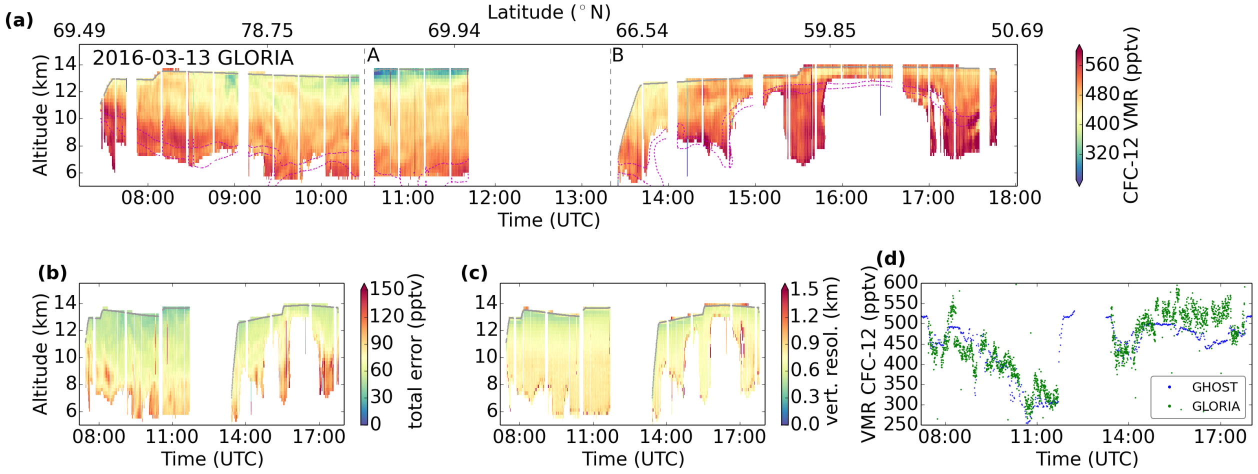

Figure 11. CFC-12 flight PGS19: Cross section of (a) retrieved CFC-12 volume mixing ratio (the flight altitude is marked with a grey line, the ECMWF potential vorticities of 2 and 4 PVU are marked with magenta dashed lines, way points are marked with grey vertical dashed lines). Cross sections of (b) total estimated error, (c) vertical resolution and (d) comparison of the GLORIA measurements (green) to the GhOST-MS in-situ measurement (blue).

for remote sensing change during the winter: In January many PSCs occur, which influence the measured infra red spectra and make temperature and trace gas retrievals challenging. Towards the end of the Arctic winter, more delicate structures in trace gases are present due to nitrification and related events, which make comparisons of measurements at different geolocations more difficult. These changing atmospheric conditions are also visible in the comparisons in Tab. 2: Deviations between GLORIA and BAHAMAS temperatures are larger for flights in January (due to the influence of PSCs). Another measure for the agreement between GLORIA and in-situ instruments is the part of co-located measurements, of which the differences are within twice the combined estimated errors of the cross-compared instruments. For temperature 88%, for HNO_3 73%, for O_3 63%, for $ClONO_2$ 53%, for H_2O 90%, for CFC-12 77%, and in total 73% of the comparisons show this agreement. $ClONO_2$, O_3, and HNO_3 show substantial variations at flight altitude (e.g. Figs. 9, 8, 7). We attribute the lower fraction of agreement to the higher atmospheric variability of those trace gases, thereby complicating the comparison due to the strongly differing instrumental sampling characteristics. MLS O_3 and HNO_3 values become increasingly smaller compared to the corresponding GLORIA measurements towards the end of the Arctic winter. This is explained by the fine structures which are visible in the GLORIA measurements, but not resolved in Aura/MLS data due to their lower vertical resolution and horizontal gridding.

5 Conclusions

We discuss ~~recent~~ a survey of recent measurements in the high spectral resolution mode of the imaging FTS limb sounder GLORIA, which was deployed on the German research aircraft HALO during the PGS field campaign in the Arctic winter

Table 2. Median differences between GLORIA and in-situ and Aura/MLS measurements with the median absolute deviation (as a measure of the spread of the difference around the median value) for each flight and the whole campaign. For the flight on 12 January 2016 (PGS06) no water vapor in-situ measurements are available.

Flight date	Temp. [K] BAHAMAS	HNO_3 [ppbv] AIMS	HNO_3 [ppbv] MLS	O_3 [ppbv] FAIRO	O_3 [ppbv] MLS	$ClONO_2$ [pptv] AIMS	H_2O [ppmv] FISH	CFC-12 [pptv] GhOST
15-12-21	-0.97 ± 0.63	0.38 ± 0.33	0.99 ± 0.35	40.5 ± 89.9	197.4 ± 86.9	20.3 ± 64.9	-0.42 ± 0.52	-21.9 ± 25.6
16-01-12	-1.15 ± 0.91	0.03 ± 0.68	1.31 ± 0.79	-123.4 ± 127.4	257.4 ± 176.7	-35.3 ± 84.5		-58.2 ± 21.7
16-01-18	-2.04 ± 1.47	0.47 ± 1.15	1.39 ± 0.82	66.6 ± 80.2	261.0 ± 149.1	-11.2 ± 75.8	-0.67 ± 0.59	-66.5 ± 50.5
16-01-20	-1.99 ± 1.21	-1.03 ± 0.80	1.41 ± 0.74	19.7 ± 129.0	266.4 ± 126.6	-33.3 ± 70.7	-0.71 ± 0.76	-44.6 ± 48.3
16-01-22	-1.09 ± 1.15	-0.10 ± 1.30	1.83 ± 0.66	-21.2 ± 108.9	365.7 ± 101.2	-11.0 ± 84.3	-0.01 ± 0.70	-55.3 ± 46.1
16-01-25	-2.18 ± 0.66	-0.82 ± 0.99	1.84 ± 0.63	4.5 ± 109.9	435.8 ± 170.3	-6.6 ± 85.3	-0.32 ± 0.49	-57.9 ± 29.4
16-01-28	-1.78 ± 0.67	-0.48 ± 0.42	1.37 ± 0.58	4.4 ± 37.8	230.4 ± 104.3	56.0 ± 78.6	-0.69 ± 0.40	-28.0 ± 13.7
16-01-31	-0.56 ± 0.60	-1.83 ± 1.52	2.26 ± 0.86	17.8 ± 76.9	397.1 ± 134.6	7.3 ± 67.6	-0.75 ± 0.52	-9.2 ± 26.2
16-02-02	-0.45 ± 0.76	0.21 ± 0.79	1.94 ± 0.72	17.0 ± 50.7	324.0 ± 123.7	-17.4 ± 60.2	0.07 ± 0.64	-17.1 ± 32.3
16-02-26	-0.98 ± 0.80	0.23 ± 0.66	2.12 ± 1.58	-42.4 ± 92.4	319.8 ± 210.3	-22.4 ± 88.9	-0.24 ± 0.68	7.6 ± 29.2
16-03-06	-0.82 ± 0.66	0.10 ± 0.48	2.46 ± 1.26	12.8 ± 68.6	387.2 ± 194.5	1.7 ± 87.4	-0.16 ± 0.68	-21.9 ± 53.6
16-03-09	-0.83 ± 0.74	-0.38 ± 0.88	2.64 ± 1.06	72.9 ± 144.2	418.3 ± 194.0	-35.0 ± 127.8	-0.05 ± 0.49	-41.8 ± 49.9
16-03-13	-0.14 ± 0.86	-0.24 ± 0.95	3.04 ± 1.10	55.7 ± 139.6	465.3 ± 225.2	-18.4 ± 202.6	0.24 ± 0.55	2.4 ± 39.6
16-03-16	-0.06 ± 0.78	0.02 ± 0.42	0.32 ± 0.53	-114.8 ± 120.1	113.2 ± 97.8	-9.9 ± 235.4	-0.06 ± 0.55	26.4 ± 41.0
16-03-18	-0.64 ± 0.98	0.69 ± 0.60	3.57 ± 0.76	60.5 ± 152.8	549.0 ± 234.4	-47.0 ± 131.5	0.19 ± 0.53	18.1 ± 34.6
Campaign	-0.75 ± 0.88	-0.03 ± 0.85	2.01 ± 1.33	-3.5 ± 116.8	346.0 ± 202.7	-15.4 ± 102.8	-0.13 ± 0.63	-19.8 ± 46.9

2015/2016. As an example, we discuss the flight PGS19 on 13 March 2016 in detail, showing the retrieval results of temperature and the trace gases HNO_3, O_3, $ClONO_2$, H_2O and CFC-12 and compare them to in-situ measurements and to MLS where applicable. We demonstrate that valuable information at high spatial resolution can be retrieved from infrared limb imaging data even in the UTLS with high clouds and PSCs present. Fine vertical structures can be examined thanks to vertical resolutions of 400 to 1000 m. Typical estimated errors are in the range of 1 - 2 K for temperature, and 10 - 20 % relative error for the discussed trace gases. An approach for post-flight LOS correction was successfully established to account for limited in-flight LOS knowledge and stabilization due to technical and software problems.

The comparisons of the MLS and GLORIA HNO_3 and O_3 measurements show the advantage of airborne measurements: The aircraft measurements with high spatial resolution reveal small-scale structures in the trace gas distributions. In contrast, the satellite measurements provide a continuous time series of global measurements up to high altitudes, which helps to put the structures observed by GLORIA into context. The qualitative comparison shows that the same structures in O_3 and HNO_3 are visible in both data sets and the measured mixing ratios are of the same order of magnitude. Towards the end of the winter, O_3 and HNO_3 are underestimated by MLS, which is an effect of lower vertical resolution of the spaceborne instrument and horizontal gridding. This lower resolution does not resolve spatially confined enhancements in these trace gases. Due to only partial overlap of vertically resolved information from GLORIA and the width of the MLS averaging kernels, it is not possible to perform a more quantitative comparison.

Comparisons of the GLORIA retrieval results with in-situ measurements on board HALO show the consistency of these data sets, taking into account the error, vertical and horizontal resolutions of GLORIA and atmospheric variability, which are pronounced by the different measurement techniques and the inferred different geolocations of the measurements.

This newly presented GLORIA data set benefits from aero-acoustic improvements of the instrument compared to a previous GLORIA campaigns (Kaufmann et al., 2015; Woiwode et al., 2015; Ungermann et al., 2015). It is based on a much higher number of measured profiles and also has been compared to additional in-situ trace gas measurements. Compared to the data set by Woiwode et al. (2015), which is also based on measurements in the high spectral resolution mode, the vertical resolutions of this GLORIA data set are significantly better and a more detailed approach for error estimation is introduced. Furthermore, GLORIA measurements discussed in the paper at hand provide temperature and trace gas information down to 5 km, which is lower compared to the majority of previously discussed infrared limb sounders, due to the much higher vertical and horizontal sampling of the limb-imaging spectrometer. In future retrieval setups we will aim to retrieve additional trace gases such as C_2H_6 and PAN.

The results demonstrate the performance and quality of this GLORIA data set of the UTLS during the Arctic winter 2015/2016. GLORIA measurements ~~of this region with rather high spatial sampling allow further~~ with unprecedented spatial resolution over the Arctic region will form the basis for many future case studies on chlorine deactivation, denitrification and mesoscale structures.

Data availability. The discussed GLORIA data set and in-situ data sets are available at the HALO database https://halo-db.pa.op.dlr.de. Aura/MLS data is available at https://mls.jpl.nasa.gov. ECMWF analysis data is available at https://www.ecmwf.int.

Competing interests. The authors declare that they have no conflict of interest.

Acknowledgements. We thank referees 1 and 2 for their valuable and detailed feedback, which helped to improve this manuscript. We gratefully thank the POLSTRACC/GW-LCYCLE II/SALSA coordination team and DLR-FX for successfully conducting the field campaign. The results are based on the efforts of all members of the GLORIA team, including the technology institutes ZEA-1 and ZEA-2 at Forschungszentrum Jülich and the Institute for Data Processing and Electronics at the Karlsruhe Institute of Technology. We thank the European Centre for Medium-Range Weather Forecasts (ECMWF) for providing their meteorological analyses. S. Johansson has received funding from the European Community's Seventh Framework Programme (FP7/2007-2013) under grant agreement 603557. A. Marsing, T. Jurkat-Witschas and C. Voigt were funded by DFG under contract number JU 3059/1-1 and VO 1504/4-1. This work was partly supported by the Bundesministerium für Bildung und Forschung (BMBF) under the project ROMIC/GW-LCYCLE, subproject 2 (01LG1206B). S. Johansson gratefully thanks the Graduate School for Climate and Environment (GRACE), Karlsruhe Institute of Technology for funding his visit to the Jet Propulsion Laboratory to discuss the comparisons with the Aura/MLS measurements and the MLS team for the hospitality during that time. Work at the Jet Propulsion Laboratory, California Institute of Technology, was done under contract with the National Aeronautics and Space Administration. This work was partly supported by the German Research Foundation (Deutsche Forschungsgemeinschaft, DFG Priority Program SPP 1294). We acknowledge support by the Deutsche Forschungsgemeinschaft and the Open Access Publishing Fund of the Karlsruhe Institute of Technology.

References

Bange, J., Esposito, M., Lenschow, D. H., Brown, P. R. A., Dreiling, V., Giez, A., Mahrt, L., Malinowski, S. P., Rodi, A. R., Shaw, R. A., Siebert, H., Smit, H., and Zöger, M.: Measurement of Aircraft State and Thermodynamic and Dynamic Variables, https://doi.org/10.1002/9783527653218.ch2, http://onlinelibrary.wiley.com/doi/10.1002/9783527653218.ch2/pdf, 2013.

Bönisch, H., Engel, A., Birner, T., Hoor, P., Tarasick, D. W., and Ray, E. A.: On the structural changes in the Brewer-Dobson circulation after 2000, Atmospheric Chemistry and Physics, 11, 3937–3948, https://doi.org/10.5194/acp-11-3937-2011, https://www.atmos-chem-phys.net/11/3937/2011/acp-11-3937-2011.pdf, 2011.

Brault, J. W.: New approach to high-precision Fourier transform spectrometer design, Applied Optics, 35, 2891–2896, https://doi.org/10.1364/AO.35.002891, https://www.osapublishing.org/viewmedia.cfm?uri=ao-35-16-2891&seq=0, 1996.

Clarmann, T., Fischer, H., Friedl-Vallon, F., Linden, A., Oelhaf, H., Piesch, C., Seefeldner, M., and Völker, W.: Retrieval of stratospheric O3, HNO3 and ClONO2 profiles from 1992 MIPAS–B limb emission spectra: Method, results, and error analysis, Journal of Geophysical Research: Atmospheres, 98, 20 495–20 506, https://doi.org/10.1029/93JD02261, http://onlinelibrary.wiley.com/doi/10.1029/93JD02261/pdf, 1993.

Eriksson, P.: Analysis and comparison of two linear regularization methods for passive atmospheric observations, Journal of Geophysical Research: Atmospheres, 105, 18 157–18 167, https://doi.org/10.1029/2000JD900172, http://onlinelibrary.wiley.com/doi/10.1029/2000JD900172/pdf, 2000.

Fahey, D. W., Kelly, K. K., Kawa, S. R., Tuck, A. F., Loewenstein, M., Chan, K. R., and Heidt, L. E.: Observations of denitrification and dehydration in the winter polar stratospheres, Nature, 344, 321, https://doi.org/10.1038/344321a0, https://www.nature.com/articles/344321a0.pdf, 1990.

Fahey, D. W., Gao, R.-S., Möhler, O., Saathoff, H., Schiller, C., Ebert, V., Krämer, M., Peter, T., Amarouche, N., Avallone, L. M., Bauer, R., Bozóki, Z., Christensen, L. E., Davis, S. M., Durry, G., Dyroff, C., Herman, R. L., Hunsmann, S., Khaykin, S. M., Mackrodt, P., Meyer, J., Smith, J. B., Spelten, N., Troy, R. F., Vömel, H., Wagner, S., and Wienhold, F. G.: The AquaVIT-1 intercomparison of atmospheric water vapor measurement techniques, Atmospheric Measurement Techniques, 7, 3177–3213, https://doi.org/10.5194/amt-7-3177-2014, https://www.atmos-meas-tech.net/7/3177/2014/amt-7-3177-2014.pdf, 2014.

Fischer, H. and Oelhaf, H.: Remote sensing of vertical profiles of atmospheric trace constituents with MIPAS limb-emission spectrometers, Applied Optics, 35, 2787–2796, https://doi.org/10.1364/AO.35.002787, https://www.osapublishing.org/viewmedia.cfm?uri=ao-35-16-2787&seq=0, 1996.

Fischer, H., Birk, M., Blom, C., Carli, B., Carlotti, M., von Clarmann, T., Delbouille, L., Dudhia, A., Ehhalt, D., Endemann, M., Flaud, J. M., Gessner, R., Kleinert, A., Koopman, R., Langen, J., López-Puertas, M., Mosner, P., Nett, H., Oelhaf, H., Perron, G., Remedios, J., Ridolfi, M., Stiller, G., and Zander, R.: MIPAS: An instrument for atmospheric and climate research, Atmospheric Chemistry and Physics, 8, 2151–2188, https://doi.org/10.5194/acp-8-2151-2008, https://www.atmos-chem-phys.net/8/2151/2008/acp-8-2151-2008.pdf, 2008.

Flaud, J.-M., Piccolo, C., and Carli, B.: A Spectroscopic Database for MIPAS, in: Proceedings of the ENVISAT validation workshop, ESRIN, Italy, 2002.

Flaud, J.-M., Brizzi, G., Carlotti, M., Perrin, A., and Ridolfi, M.: MIPAS database: Validation of HNO₃ line parameters using MIPAS satellite measurements, Atmospheric Chemistry and Physics, 6, 5037–5048, https://doi.org/10.5194/acp-6-5037-2006, https://www.atmos-chem-phys.net/6/5037/2006/acp-6-5037-2006.pdf, 2006.

Friedl-Vallon, F., Maucher, G., Seefeldner, M., Trieschmann, O., Kleinert, A., Lengel, A., Keim, C., Oelhaf, H., and Fischer, H.: Design and characterization of the balloon-borne Michelson Interferometer for Passive Atmospheric Sounding (MIPAS-B2), Applied Optics, 43, 3335–3355, https://doi.org/10.1364/AO.43.003335, https://www.osapublishing.org/viewmedia.cfm?uri=ao-43-16-3335&seq=0, 2004.

Friedl-Vallon, F., Gulde, T., Hase, F., Kleinert, A., Kulessa, T., Maucher, G., Neubert, T., Olschewski, F., Piesch, C., Preusse, P., Rongen, H., Sartorius, C., Schneider, H., Schönfeld, A., Tan, V., Bayer, N., Blank, J., Dapp, R., Ebersoldt, A., Fischer, H., Graf, F., Guggenmoser, T., Höpfner, M., Kaufmann, M., Kretschmer, E., Latzko, T., Nordmeyer, H., Oelhaf, H., Orphal, J., Riese, M., Schardt, G., Schillings, J., Sha, M. K., Suminska-Ebersoldt, O., and Ungermann, J.: Instrument concept of the imaging Fourier transform spectrometer GLORIA, Atmospheric Measurement Techniques, 7, 3565–3577, https://doi.org/10.5194/amt-7-3565-2014, 2014.

Froidevaux, L., Jiang, Y. B., Lambert, A., Livesey, N. J., Read, W. G., Waters, J. W., Browell, E. V., Hair, J. W., Avery, M. A., McGee, T. J., Twigg, L. W., Sumnicht, G. K., Jucks, K. W., Margitan, J. J., Sen, B., Stachnik, R. A., Toon, G. C., Bernath, P. F., Boone, C. D., Walker, K. A., Filipiak, M. J., Harwood, R. S., Fuller, R. A., Manney, G. L., Schwartz, M. J., Daffer, W. H., Drouin, B. J., Cofield, R. E., Cuddy, D. T., Jarnot, R. F., Knosp, B. W., Perun, V. S., Snyder, W. V., Stek, P. C., Thurstans, R. P., and Wagner, P. A.: Validation of Aura Microwave Limb Sounder stratospheric ozone measurements, Journal of Geophysical Research: Atmospheres, 113, https://doi.org/10.1029/2007JD008771, http://onlinelibrary.wiley.com/doi/10.1029/2007JD008771/full, 2008.

Gettelman, A., Hoor, P., Pan, L. L., Randel, W. J., Hegglin, M. I., and Birner, T.: THE EXTRATROPICAL UPPER TROPOSPHERE AND LOWER STRATOSPHERE, Reviews of Geophysics, 49, https://doi.org/10.1029/2011RG000355, 2011.

Giez, A., Mallaun, C., Zöger, M., Dörnbrack, A., and Schumann, U.: Static Pressure from Aircraft Trailing-Cone Measurements and Numerical Weather-Prediction Analysis, Journal of Aircraft, 54, 1728–1737, https://doi.org/10.2514/1.C034084, 2017.

Greenblatt, J. B., Jost, H.-J., Loewenstein, M., Podolske, J. R., Bui, T. P., Hurst, D. F., Elkins, J. W., Herman, R. L., Webster, C. R., Schauffler, S. M., Atlas, E. L., Newman, P. A., Lait, L. R., Müller, M., Engel, A., and Schmidt, U.: Defining the polar vortex edge from an N2O:potential temperature correlation, Journal of Geophysical Research: Atmospheres, 107, https://doi.org/10.1029/2001JD000575, http://onlinelibrary.wiley.com/doi/10.1029/2001JD000575/full, 2002.

Guggenmoser, T., Blank, J., Kleinert, A., Latzko, T., Ungermann, J., Friedl-Vallon, F., Höpfner, M., Kaufmann, M., Kretschmer, E., Maucher, G., Neubert, T., Oelhaf, H., Preusse, P., Riese, M., Rongen, H., Sha, M. K., Sumińska-Ebersoldt, O., and Tan, V.: New calibration noise suppression techniques for the GLORIA limb imager, Atmospheric Measurement Techniques, 8, 3147–3161, https://doi.org/10.5194/amt-8-3147-2015, https://www.atmos-meas-tech.net/8/3147/2015/amt-8-3147-2015.pdf, 2015.

Holton, J. R., Haynes, P. H., McIntyre, M. E., Douglass, A. R., Rood, R. B., and Pfister, L.: Stratosphere–troposphere exchange, Reviews of Geophysics, 33, 403–439, https://doi.org/10.1029/95RG02097, http://onlinelibrary.wiley.com/doi/10.1029/95RG02097/pdf, 1995.

Höpfner, M.: Derivatives and interface to the retrieval, in: The Karlsruhe Optimized and Precise Radiative transfer Algorithm (KOPRA), edited by Stiller, G. P., Wissenschaftliche Berichte, pp. 133–144, Forschungszentrum Karlsruhe, 2000.

Jiang, Y. B., Froidevaux, L., Lambert, A., Livesey, N. J., Read, W. G., Waters, J. W., Bojkov, B., Leblanc, T., McDermid, I. S., Godin-Beekmann, S., Filipiak, M. J., Harwood, R. S., Fuller, R. A., Daffer, W. H., Drouin, B. J., Cofield, R. E., Cuddy, D. T., Jarnot, R. F., Knosp, B. W., Perun, V. S., Schwartz, M. J., Snyder, W. V., Stek, P. C., Thurstans, R. P., Wagner, P. A., Allaart, M., Andersen, S. B., Bodeker, G., Calpini, B., Claude, H., Coetzee, G., Davies, J., de Backer, H., Dier, H., Fujiwara, M., Johnson, B., Kelder, H., Leme, N. P., König-Langlo, G., Kyro, E., Laneve, G., Fook, L. S., Merrill, J., Morris, G., Newchurch, M., Oltmans, S., Parrondos, M. C., Posny, F., Schmidlin, F., Skrivankova, P., Stubi, R., Tarasick, D., Thompson, A., Thouret, V., Viatte, P., Vömel, H., von der Gathen, P., Yela, M., and Zablocki, G.: Validation of Aura Microwave Limb Sounder Ozone by ozonesonde and lidar measurements, Journal of Geophysical Research: Atmospheres, 112, https://doi.org/10.1029/2007JD008776, http://onlinelibrary.wiley.com/doi/10.1029/2007JD008776/full, 2007.

Jurkat, T., Kaufmann, S., Voigt, C., Schäuble, D., Jeßberger, P., and Ziereis, H.: The airborne mass spectrometer AIMS – Part 2: Measurements of trace gases with stratospheric or tropospheric origin in the UTLS, Atmospheric Measurement Techniques, 9, 1907–1923, https://doi.org/10.5194/amt-9-1907-2016, https://www.atmos-meas-tech.net/9/1907/2016/amt-9-1907-2016.pdf, 2016.

Jurkat, T., Voigt, C., Kaufmann, S., Grooß, J.-U., Ziereis, H., Dörnbrack, A., Hoor, P., Bozem, H., Engel, A., Bönisch, H., Keber, T., Hüneke, T., Pfeilsticker, K., Zahn, A., Walker, K. A., Boone, C. D., Bernath, P. F., and Schlager, H.: Depletion of ozone and reservoir species of chlorine and nitrogen oxide in the lower Antarctic polar vortex measured from aircraft, Geophysical Research Letters, 44, 6440–6449, https://doi.org/10.1002/2017GL073270, http://onlinelibrary.wiley.com/doi/10.1002/2017GL073270/full, 2017.

Kaufmann, M., Blank, J., Guggenmoser, T., Ungermann, J., Engel, A., Ern, M., Friedl-Vallon, F., Gerber, D., Grooß, J. U., Guenther, G., Höpfner, M., Kleinert, A., Kretschmer, E., Latzko, T., Maucher, G., Neubert, T., Nordmeyer, H., Oelhaf, H., Olschewski, F., Orphal, J., Preusse, P., Schlager, H., Schneider, H., Schuettemeyer, D., Stroh, F., Suminska-Ebersoldt, O., Vogel, B., M. Volk, C., Woiwode, W., and Riese, M.: Retrieval of three-dimensional small-scale structures in upper-tropospheric/lower-stratospheric composition as measured by GLORIA, Atmospheric Measurement Techniques, 8, 81–95, https://doi.org/10.5194/amt-8-81-2015, https://www.atmos-meas-tech.net/8/81/2015/amt-8-81-2015.pdf, 2015.

Kaufmann, S., Voigt, C., Jurkat, T., Thornberry, T., Fahey, D. W., Gao, R.-S., Schlage, R., Schäuble, D., and Zöger, M.: The airborne mass spectrometer AIMS – Part 1: AIMS-H₂O for UTLS water vapor measurements, Atmospheric Measurement Techniques, 9, 939–953, https://doi.org/10.5194/amt-9-939-2016, https://www.atmos-meas-tech.net/9/939/2016/amt-9-939-2016.pdf, 2016.

Khosrawi, F., Kirner, O., Sinnhuber, B.-M., Johansson, S., Höpfner, M., Santee, M. L., Froidevaux, L., Ungermann, J., Ruhnke, R., Woiwode, W., Oelhaf, H., and Braesicke, P.: Denitrification, dehydration and ozone loss during the 2015/2016 Arctic winter, Atmospheric Chemistry and Physics, 17, 12 893–12 910, https://doi.org/10.5194/acp-17-12893-2017, https://www.atmos-chem-phys.net/17/12893/2017/acp-17-12893-2017.pdf, 2017.

Kleinert, A., Friedl-Vallon, F., Guggenmoser, T., Höpfner, M., Neubert, T., Ribalda, R., Sha, M. K., Ungermann, J., Blank, J., Ebersoldt, A., Kretschmer, E., Latzko, T., Oelhaf, H., Olschewski, F., and Preusse, P.: Level 0 to 1 processing of the imaging Fourier transform spectrometer GLORIA: Generation of radiometrically and spectrally calibrated spectra, Atmospheric Measurement Techniques, 7, 4167–4184, https://doi.org/10.5194/amt-7-4167-2014, 2014.

Konopka, P. and Pan, L. L.: On the mixing–driven formation of the Extratropical Transition Layer (ExTL), Journal of Geophysical Research: Atmospheres, 117, https://doi.org/10.1029/2012JD017876, http://onlinelibrary.wiley.com/doi/10.1029/2012JD017876/full, 2012.

Krautstrunk, M. and Giez, A.: The Transition From FALCON to HALO Era Airborne Atmospheric Research, in: Atmospheric physics, edited by Schumann, U., Research topics in aerospace, pp. 609–624, Springer, Berlin, https://doi.org/10.1007/978-3-642-30183-4_37, 2012.

Kretschmer, E., Bachner, M., Blank, J., Dapp, R., Ebersoldt, A., Friedl-Vallon, F., Guggenmoser, T., Gulde, T., Hartmann, V., Lutz, R., Maucher, G., Neubert, T., Oelhaf, H., Preusse, P., Schardt, G., Schmitt, C., Schönfeld, A., and Tan, V.: In-flight control and communication architecture of the GLORIA imaging limb sounder on atmospheric research aircraft, Atmospheric Measurement Techniques, 8, 2543–2553, https://doi.org/10.5194/amt-8-2543-2015, https://www.atmos-meas-tech.net/8/2543/2015/amt-8-2543-2015.pdf, 2015.

Krisch, I., Preusse, P., Ungermann, J., Dörnbrack, A., Eckermann, S. D., Ern, M., Friedl-Vallon, F., Kaufmann, M., Oelhaf, H., Rapp, M., Strube, C., and Riese, M.: First tomographic observations of gravity waves by the infrared limb imager GLORIA, Atmospheric Chemistry and Physics, 17, 14 937–14 953, https://doi.org/10.5194/acp-17-14937-2017, https://www.atmos-chem-phys.net/17/14937/2017/acp-17-14937-2017.pdf, 2017.

Livesey, N. J., Read, W. G., Wagner, P. A., Froidevaux, L., Lambert, A., Manney, G. L., Millán, L. F., Pumphrey, Hugh, C., Santee, M. L., Schwartz, M. J., Wang, S., Fuller, R. A., Jarnot, R. F., Knosp, B. W., and Martinez, E.: Version 4.2x Level 2 data quality and description document. Earth Observing System (EOS) Aura Microwave Limb Sounder (MLS), https://mls.jpl.nasa.gov/data/v4-2_data_quality_document.pdf, 2017.

Meyer, J., Rolf, C., Schiller, C., Rohs, S., Spelten, N., Afchine, A., Zöger, M., Sitnikov, N., Thornberry, T. D., Rollins, A. W., Bozóki, Z., Tátrai, D., Ebert, V., Kühnreich, B., Mackrodt, P., Möhler, O., Saathoff, H., Rosenlof, K. H., and Krämer, M.: Two decades of water vapor measurements with the FISH fluorescence hygrometer: A review, Atmospheric Chemistry and Physics, 15, 8521–8538, https://doi.org/10.5194/acp-15-8521-2015, https://www.atmos-chem-phys.net/15/8521/2015/acp-15-8521-2015.pdf, 2015.

Moore, D. P., Waterfall, A. M., and Remedios, J. J.: The potential for radiometric retrievals of halocarbon concentrations from the MIPAS-E instrument, Advances in Space Research, 37, 2238–2246, https://doi.org/10.1016/j.asr.2005.06.058, /science/article/pii/S0273117705008859/pdfft?md5=97b734fcac1495eb3668b3fe6926b4bc&pid=1-s2.0-S0273117705008859-main.pdf, 2006.

Nash, E. R., Newman, P. A., Rosenfield, J. E., and Schoeberl, M. R.: An objective determination of the polar vortex using Ertel's potential vorticity, Journal of Geophysical Research: Atmospheres (1984–2012), 101, 9471–9478, https://doi.org/10.1029/96JD00066, http://onlinelibrary.wiley.com/doi/10.1029/96JD00066/pdf, 1996.

Norton, R. H. and Beer, R.: New apodizing functions for Fourier spectrometry, JOSA, 66, 259–264, https://doi.org/10.1364/JOSA.66.000259, https://www.osapublishing.org/viewmedia.cfm?uri=josa-66-3-259&seq=0, 1976.

Norton, R. H. and Beer, R.: Errata: New Apodizing Functions For Fourier Spectrometry, JOSA, 67, 419, https://doi.org/10.1364/JOSA.67.000419, https://www.osapublishing.org/viewmedia.cfm?uri=josa-67-3-419&seq=0, 1977.

Obersteiner, F., Bönisch, H., and Engel, A.: An automated gas chromatography time-of-flight mass spectrometry instrument for the quantitative analysis of halocarbons in air, Atmospheric Measurement Techniques, 9, 179–194, https://doi.org/10.5194/amt-9-179-2016, https://www.atmos-meas-tech.net/9/179/2016/amt-9-179-2016.pdf, 2016.

Oelhaf, H., v. Clarmann, T., Fischer, H., Friedl-Vallon, F., Fritzsche, C., Linden, A., Piesch, C., Seefeldner, M., and Völker, W.: Stratospheric ClONO2 and HNO3 profiles inside the Arctic vortex from MIPAS–B limb emission spectra obtained during EASOE, Geophysical Research Letters, 21, 1263–1266, https://doi.org/10.1029/93GL01303, http://onlinelibrary.wiley.com/doi/10.1029/93GL01303/pdf, 1994.

Oelhaf, H., Sinnhuber, B.-M., and Woiwode, W.: POLSTRACC - POLar STRAtosphere in a Changing Climate, https://www.polstracc.kit.edu/, 2015.

Offermann, D., Grossmann, K.-U., Barthol, P., Knieling, P., Riese, M., and Trant, R.: Cryogenic Infrared Spectrometers and Telescopes for the Atmosphere (CRISTA) experiment and middle atmosphere variability, Journal of Geophysical Research: Atmospheres, 104, 16 311–16 325, https://doi.org/10.1029/1998JD100047, http://onlinelibrary.wiley.com/doi/10.1029/1998JD100047/pdf, 1999.

Olschewski, F., Ebersoldt, A., Friedl-Vallon, F., Gutschwager, B., Hollandt, J., Kleinert, A., Monte, C., Piesch, C., Preusse, P., Rolf, C., Steffens, P., and Koppmann, R.: The in-flight blackbody calibration system for the GLORIA interferometer on board an airborne research platform, Atmospheric Measurement Techniques, 6, 3067–3082, https://doi.org/10.5194/amt-6-3067-2013, https://www.atmos-meas-tech.net/6/3067/2013/amt-6-3067-2013.pdf, 2013.

Peter, T. and Grooß, J.-U.: Chapter 4: Polar Stratospheric Clouds and Sulfate Aerosol Particles: Microphysics, Denitrification and Heterogeneous Chemistry, https://doi.org/10.1039/9781849733182-00108, http://pubs.rsc.org/en/content/chapterpdf/2011/bk9781849730020-00108?isbn=978-1-84973-002-0&sercode=bk, 2011.

Phillips, D. L.: A Technique for the Numerical Solution of Certain Integral Equations of the First Kind, Journal of the ACM (JACM), 9, 84–97, https://doi.org/10.1145/321105.321114, http://dl.acm.org/ft_gateway.cfm?id=321114&type=pdf, 1962.

Piesch, C., Gulde, T., Sartorius, C., Friedl-Vallon, F., Seefeldner, M., Wölfel, M., Blom, C. E., and Fischer, H., eds.: Design of a MIPAS instrument for high-altitude aircraft, Proc. of the 2nd Internat. Airborne Remote Sensing Conference and Exhibition, 1996.

Piesch, C., Sartorius, C., Friedl-Vallon, F., Gulde, T., Heger, S., Kretschmer, E., Maucher, G., Nordmeyer, H., Barthel, J., Ebersoldt, A., Graf, F., Hase, F., Kleinert, A., Neubert, T., and Schillings, H. J.: The mechanical and thermal setup of the GLORIA spectrometer, Atmospheric Measurement Techniques, 8, 1773–1787, https://doi.org/10.5194/amt-8-1773-2015, https://www.atmos-meas-tech.net/8/1773/2015/amt-8-1773-2015.pdf, 2015.

Popp, P. J., Marcy, T. P., Gao, R. S., Watts, L. A., Fahey, D. W., Richard, E. C., Oltmans, S. J., Santee, M. L., Livesey, N. J., Froidevaux, L., Sen, B., Toon, G. C., Walker, K. A., Boone, C. D., and Bernath, P. F.: Stratospheric correlation between nitric acid and ozone, Journal of Geophysical Research: Atmospheres, 114, https://doi.org/10.1029/2008JD010875, https://agupubs.onlinelibrary.wiley.com/doi/full/10.1029/2008JD010875, 2009.

Remedios, J. J., Leigh, R. J., Waterfall, A. M., Moore, D. P., Sembhi, H., Parkes, I., Greenhough, J., Chipperfield, M. P., and Hauglustaine, D.: MIPAS reference atmospheres and comparisons to V4.61/V4.62 MIPAS level 2 geophysical data sets, Atmospheric Chemistry and Physics Discussions, pp. 9973–10 017, https://doi.org/10.5194/acpd-7-9973-2007, https://www.atmos-chem-phys-discuss.net/acpd-2007-0225/acpd-7-9973-2007.pdf, 2007.

Revercomb, H. E., Buijs, H., Howell, H. B., LaPorte, D. D., Smith, W. L., and Sromovsky, L. A.: Radiometric calibration of IR Fourier transform spectrometers: Solution to a problem with the High-Resolution Interferometer Sounder, Applied Optics, 27, 3210–3218, https://doi.org/10.1364/AO.27.003210, https://www.osapublishing.org/viewmedia.cfm?uri=ao-27-15-3210&seq=0, 1988.

Riese, M., Oelhaf, H., Preusse, P., Blank, J., Ern, M., Friedl-Vallon, F., Fischer, H., Guggenmoser, T., Höpfner, M., Hoor, P., Kaufmann, M., Orphal, J., Plöger, F., Spang, R., Suminska-Ebersoldt, O., Ungermann, J., Vogel, B., and Woiwode, W.: Gimballed Limb Observer for Radiance Imaging of the Atmosphere (GLORIA) scientific objectives, Atmospheric Measurement Techniques, 7, 1915–1928, https://doi.org/10.5194/amt-7-1915-2014, 2014.

Roche, A. E., Kumer, J. B., Mergenthaler, J. L., Nightingale, R. W., Uplinger, W. G., Ely, G. A., Potter, J. F., Wuebbles, D. J., Connell, P. S., and Kinnison, D. E.: Observations of Lower-Stratospheric ClONO 2 , HNO 3 , and Aerosol by the UARS CLAES Experiment between January 1992 and April 1993, Journal of the Atmospheric Sciences, 51, 2877–2902, https://doi.org/10.1175/1520-0469(1994)051<2877:OOLSCH>2.0.CO;2, 1994.

Rodgers, C. D.: Inverse Methods for Atmospheric Sounding, WORLD SCIENTIFIC, https://doi.org/10.1142/3171, 2000.

Rolf, C., Afchine, A., Bozem, H., Buchholz, B., Ebert, V., Guggenmoser, T., Hoor, P., Konopka, P., Kretschmer, E., Müller, S., Schlager, H., Spelten, N., Sumińska-Ebersoldt, O., Ungermann, J., Zahn, A., and Krämer, M.: Transport of Antarctic stratospheric strongly dehydrated air into the troposphere observed during the HALO-ESMVal campaign 2012, Atmospheric Chemistry and Physics, 15, 9143–9158, https://doi.org/10.5194/acp-15-9143-2015, https://www.atmos-chem-phys.net/15/9143/2015/acp-15-9143-2015.pdf, 2015.

Rousseeuw, P. J. and Croux, C.: Alternatives to the Median Absolute Deviation, Journal of the American Statistical Association, 88, 1273–1283, https://doi.org/10.1080/01621459.1993.10476408, 1993.

Santee, M. L., Lambert, A., Read, W. G., Livesey, N. J., Cofield, R. E., Cuddy, D. T., Daffer, W. H., Drouin, B. J., Froidevaux, L., Fuller, R. A., Jarnot, R. F., Knosp, B. W., Manney, G. L., Perun, V. S., Snyder, W. V., Stek, P. C., Thurstans, R. P., Wagner, P. A., Waters, J. W., Muscari, G., de Zafra, R. L., Dibb, J. E., Fahey, D. W., Popp, P. J., Marcy, T. P., Jucks, K. W., Toon, G. C., Stachnik, R. A., Bernath, P. F., Boone, C. D., Walker, K. A., Urban, J., and Murtagh, D.: Validation of the Aura Microwave Limb Sounder HNO3 measurements, Journal of Geophysical Research: Atmospheres, 112, https://doi.org/10.1029/2007JD008721, http://onlinelibrary.wiley.com/doi/10.1029/2007JD008721/full, 2007.

Shapiro, M. A.: Turbulent Mixing within Tropopause Folds as a Mechanism for the Exchange of Chemical Constituents between the Stratosphere and Troposphere, Journal of the Atmospheric Sciences, 37, 994–1004, https://doi.org/10.1175/1520-0469(1980)037<0994:TMWTFA>2.0.CO;2, 1980.

Spang, R., Remedios, J. J., and Brarkley, M. P.: Colour indices for the detection and differentiation of cloud types in infra-red limb emission spectra, Advances in Space Research, 33, 1041–1047, https://doi.org/10.1016/S0273-1177(03)00585-4, /science/article/pii/S0273117703005854/pdfft?md5=1e01c4a59e7a98f03118799b17f4e0a1&pid=1-s2.0-S0273117703005854-main.pdf, 2004.

Stiller, G. P., ed.: The Karlsruhe Optimized and Precise Radiative transfer Algorithm (KOPRA), vol. FZKA 6487 of *Wissenschaftliche Berichte*, Forschungszentrum Karlsruhe, 2000.

Tikhonov, A. N. and Arsenin, V. I.: Solutions of ill-posed problems, Scripta series in mathematics, Winston and Distributed solely by Halsted Press, Washington and New York, 1977.

Ungermann, J., Blank, J., Lotz, J., Leppkes, K., Hoffmann, L., Guggenmoser, T., Kaufmann, M., Preusse, P., Naumann, U., and Riese, M.: A 3-D tomographic retrieval approach with advection compensation for the air-borne limb-imager GLORIA, Atmospheric Measurement Techniques, 4, 2509–2529, https://doi.org/10.5194/amt-4-2509-2011, https://www.atmos-meas-tech.net/4/2509/2011/amt-4-2509-2011.pdf, 2011.

Ungermann, J., Kalicinsky, C., Olschewski, F., Knieling, P., Hoffmann, L., Blank, J., Woiwode, W., Oelhaf, H., Hösen, E., Volk, C. M., Ulanovsky, A., Ravegnani, F., Weigel, K., Stroh, F., and Riese, M.: CRISTA-NF measurements with unprecedented vertical resolution during the RECONCILE aircraft campaign, Atmospheric Measurement Techniques, 5, 1173–1191, https://doi.org/10.5194/amt-5-1173-2012, https://www.atmos-meas-tech.net/5/1173/2012/amt-5-1173-2012.pdf, 2012.

Ungermann, J., Blank, J., Dick, M., Ebersoldt, A., Friedl-Vallon, F., Giez, A., Guggenmoser, T., Höpfner, M., Jurkat, T., Kaufmann, M., Kaufmann, S., Kleinert, A., Krämer, M., Latzko, T., Oelhaf, H., Olchewski, F., Preusse, P., Rolf, C., Schillings, J., Suminska-Ebersoldt, O., Tan, V., Thomas, N., Voigt, C., Zahn, A., Zöger, M., and Riese, M.: Level 2 processing for the imaging Fourier transform spectrometer GLORIA: Derivation and validation of temperature and trace gas volume mixing ratios from calibrated dynamics mode spectra, Atmospheric Measurement Techniques, 8, 2473–2489, https://doi.org/10.5194/amt-8-2473-2015, https://www.atmos-meas-tech.net/8/2473/2015/amt-8-2473-2015.pdf, 2015.

Voigt, C., Dörnbrack, A., Wirth, M., Groß, S. M., Pitts, M. C., Poole, L. R., Baumann, R., Ehard, B., Sinnhuber, B.-M., Woiwode, W., and Oelhaf, H.: Widespread polar stratospheric ice clouds in the 2015/2016 Arctic winter – Implications for ice nucleation, Atmospheric Chemistry and Physics Discussions, pp. 1–29, https://doi.org/10.5194/acp-2017-1044, 2017.

von Clarmann, T., Glatthor, N., Grabowski, U., Höpfner, M., Kellmann, S., Kiefer, M., Linden, A., Tsidu, G. M., Milz, M., Steck, T., Stiller, G. P., Wang, D. Y., Fischer, H., Funke, B., Gil-López, S., and López-Puertas, M.: Retrieval of temperature and tangent altitude pointing from limb emission spectra recorded from space by the Michelson Interferometer for Passive Atmospheric Sounding (MIPAS), Journal of Geophysical Research: Atmospheres, 108, https://doi.org/10.1029/2003JD003602, http://onlinelibrary.wiley.com/doi/10.1029/2003JD003602/full, 2003.

Wagner, G. and Birk, M.: New infrared spectroscopic database for chlorine nitrate, Journal of Quantitative Spectroscopy and Radiative Transfer, 82, 443–460, https://doi.org/10.1016/S0022-4073(03)00169-9, /science/article/pii/S0022407303001699/pdfft?md5=69d7103911911a087711478fdee2a452&pid=1-s2.0-S0022407303001699-main.pdf, 2003.

Waters, J. W., Froidevaux, L., Harwood, R. S., Jarnot, R. F., Pickett, H. M., Read, W. G., Siegel, P. H., Cofield, R. E., Filipiak, M. J., Flower, D. A., Holden, J. R., Lau, G. K., Livesey, N. J., Manney, G. L., Pumphrey, H. C., Santee, M. L., Wu, D. L., Cuddy, D. T., Lay, R. R., Loo, M. S., Perun, V. S., Schwartz, M. J., Stek, P. C., Thurstans, R. P., Boyles, M. A., Chandra, K. M., Chavez, M. C., Chen, G.-S., Chudasama,

B. V., Dodge, R., Fuller, R. A., Girard, M. A., Jiang, J. H., Jiang, Y., Knosp, B. W., LaBelle, R. C., Lam, J. C., Lee, K. A., Miller, D., Oswald, J. E., Patel, N. C., Pukala, D. M., Quintero, O., Scaff, D. M., van Snyder, W., Tope, M. C., Wagner, P. A., and Walch, M. J.: The Earth observing system microwave limb sounder (EOS MLS) on the aura Satellite, IEEE Transactions on Geoscience and Remote Sensing, 44, 1075–1092, https://doi.org/10.1109/TGRS.2006.873771, 2006.

Wetzel, G., Oelhaf, H., Ruhnke, R., Friedl-Vallon, F., Kleinert, A., Kouker, W., Maucher, G., Reddmann, T., Seefeldner, M., Stowasser, M., Trieschmann, O., von Clarmann, T., and Fischer, H.: NOy partitioning and budget and its correlation with N2O in the Arctic vortex and in summer midlatitudes in 1997, Journal of Geophysical Research: Atmospheres, 107, https://doi.org/10.1029/2001JD000916, http://onlinelibrary.wiley.com/doi/10.1029/2001JD000916/full, 2002.

WMO, ed.: Scientific assessment of Ozone depletion: 2014. Pursuant to Article 6 of the Montreal Protocol on substances that deplete the ozone layer, vol. 55 of *Report / World Meteorological Organization, Global Ozone Research and Monitoring Project*, World Meteorological Organization, Geneva, http://www.wmo.int/pages/prog/arep/gaw/ozone_2014/documents/Full_report_2014_Ozone_Assessment.pdf, 2015.

Woiwode, W., Oelhaf, H., Gulde, T., Piesch, C., Maucher, G., Ebersoldt, A., Keim, C., Höpfner, M., Khaykin, S., Ravegnani, F., Ulanovsky, A. E., Volk, C. M., Hösen, E., Dörnbrack, A., Ungermann, J., Kalicinsky, C., and Orphal, J.: MIPAS-STR measurements in the Arctic UTLS in winter/spring 2010: Instrument characterization, retrieval and validation, Atmospheric Measurement Techniques, 5, 1205–1228, https://doi.org/10.5194/amt-5-1205-2012, 2012.

Woiwode, W., Sumińska-Ebersoldt, O., Oelhaf, H., Höpfner, M., Belyaev, G. V., Ebersoldt, A., Friedl-Vallon, F., Grooß, J.-U., Gulde, T., Kaufmann, M., Kleinert, A., Krämer, M., Kretschmer, E., Kulessa, T., Maucher, G., Neubert, T., Piesch, C., Preusse, P., Riese, M., Rongen, H., Sartorius, C., Schardt, G., Schönfeld, A., Schuettemeyer, D., Sha, M. K., Stroh, F., Ungermann, J., Volk, C. M., and Orphal, J.: Validation of first chemistry mode retrieval results from the new limb-imaging FTS GLORIA with correlative MIPAS-STR observations, Atmospheric Measurement Techniques, 8, 2509–2520, https://doi.org/10.5194/amt-8-2509-2015, https://www.atmos-meas-tech.net/8/2509/2015/amt-8-2509-2015.pdf, 2015.

Zahn, A., Weppner, J., Widmann, H., Schlote-Holubek, K., Burger, B., Kühner, T., and Franke, H.: A fast and precise chemiluminescence ozone detector for eddy flux and airborne application, Atmospheric Measurement Techniques, 5, 363–375, https://doi.org/10.5194/amt-5-363-2012, https://www.atmos-meas-tech.net/5/363/2012/amt-5-363-2012.pdf, 2012.

Zöger, M., Afchine, A., Eicke, N., Gerhards, M.-T., Klein, E., McKenna, D. S., Mörschel, U., Schmidt, U., Tan, V., Tuitjer, F., Woyke, T., and Schiller, C.: Fast in situ stratospheric hygrometers: A new family of balloon–borne and airborne Lyman alpha photofragment fluorescence hygrometers, Journal of Geophysical Research: Atmospheres, 104, 1807–1816, https://doi.org/10.1029/1998JD100025, http://onlinelibrary.wiley.com/doi/10.1029/1998JD100025/pdf, 1999.